REPROGRAMMING AND MODELING GLIAL ENCAPSULATION SURROUNDING IMPLANTED ELECTRODES

By

Bailey Winter

A THESIS

Submitted to
Michigan State University
in partial fulfillment of the requirements
for the degree of

Biomedical Engineering – Master of Science

2019

ABSTRACT

REPROGRAMMING AND MODELING GLIAL ENCAPSULATION SURROUNDING IMPLANTED ELECTRODES

By

Bailey Winter

Implanted microelectrode arrays are increasingly popular tools to study neural function and structure and show great promise as treatments for neurological disorders. However, these devices, especially those designed to record neural activity, often fail over time. The loss of neurons at the device-tissue interface during the reactive immune response to implantation is thought to contribute to device failure, however, the exact mechanisms are not well understood. In this thesis, I explore means of restoring the neuronal population through the direct reprogramming of astrocytes using viral vectors *in vitro*. To apply these findings to implanted microelectrodes, vectors need to be delivered to the interfacial region. To address this, a method, detailed in this thesis, has been developed to deliver vectors using microfluidic devices. Finally, the frame work for an in vitro model of the foreign body response has been constructed, with the intention of using this model to further explore the molecular pathways that are critical for propagating the foreign body response, contributing to neuronal loss, and ultimately causing device failure.

ACKNOWLEDGEMENTS

I would like to thank Dr. Erin Purcell for her support and guidance during these past few years. Without her excellent mentorship, this research would not have been possible. I would also like to thank the members of the lab. You've made this an amazing, fun, and joyous experience.

TABLE OF CONTENTS

LIST OF FIGURES

INTRODUCTION

Motivation

Microelectrode arrays (MEAs) are capable of recording the extracellular electrochemical changes associated with neural activity. This technology has proven invaluable to study the nervous system, allowing researchers to record single unit activity in both anesthetized and awake animals. MEAs have also shown great promise in clinical applications. For example, deep brain stimulation (DBS) can alleviate dyskinesia symptoms more effectively than current pharmaceutical treatments(Weaver et al. 2009; Rosin et al. 2011). Additionally, DBS has shown some initial success for patients with treatment-resistant epilepsy and depression(Mayberg et al. 2005; Halpern et al. 2009; Malone et al. 2009). Furthermore, MEAs implanted in the motor cortex of quadriplegic patients have enabled the control over robotic prostheses via brain computer interfaces(Collinger et al. 2013; Bouton et al. 2016). While these successes make a compelling case for the use of MEAs in both research and clinical settings, these devices often fail over time.

The foreign body response is thought to contribute to device failure, however, the exact mechanisms are not well understood. Furthermore, the exact mechanisms of the foreign body response are not fully characterized. During my initial project was to modify MATLAB code to more accurately quantify fluorescence expression around implanted MEAs, comparisons between vesicular γ-aminobutyric acid transporter (VGAT) and glial fibrillary acidic protein (GFAP) staining revealed the presence of VGAT positive astrocytes (Fig. 1, from my co-authored article published in the *Journal of Neurophysiology*). This suggests that astrocyte activation does not take on a singular form, but rather is a multifaceted response to injury and includes unique subtypes. Understanding this reactive immune response could elucidate mechanisms of device failure and provide a framework for extending device lifetime.

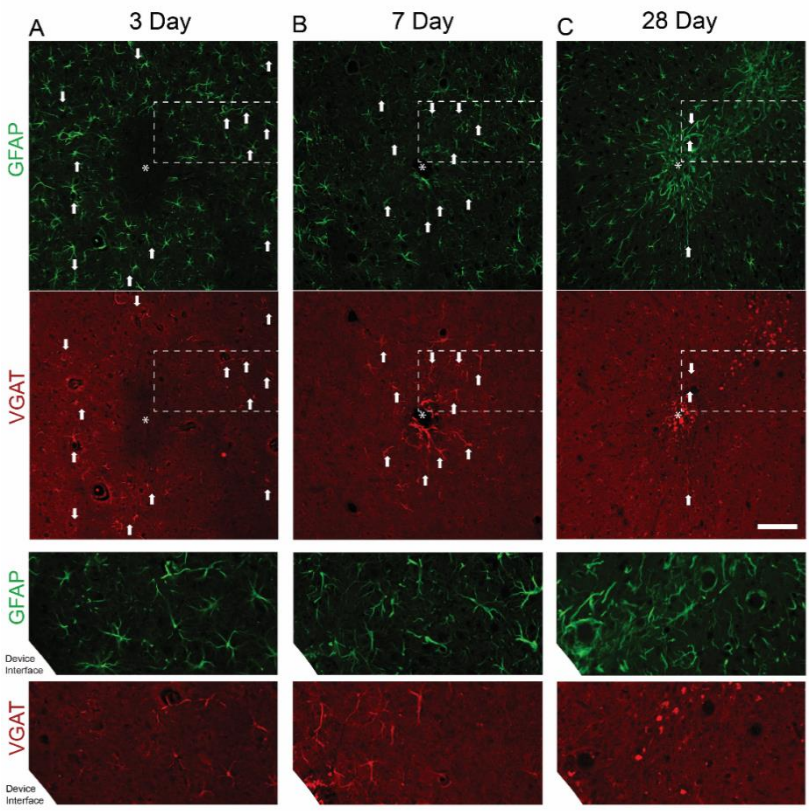

Figure 1. Reactive astroglial subtype contributes to elevated VGAT over time. (A) At 3 days, VGAT+ astroglia first emerge distal to the device interface, where arrows indicate examples of GFAP+/VGAT+ astroglia. (B) By 7 days, VGAT+ astroglia have encased the device interface. (C) After 28 days, VGAT+ astroglia are scarce, with faint exceptions indicated by arrows. White asterisks (*) denote injury sites. Scale bar = 100 μm. Device interface indicated in magnified views in bottom panels (+). Published in(Salatino et al. 2017b).

Cells contributing to the foreign body response

Two cell types that play a pivotal role in the neural tissue response to implantation are astrocytes and microglia(Polikov et al. 2005; He and Bellamkonda 2008; Salatino et al. 2017a). Astrocytes normally exhibit a star-like morphology with fine cellular processes. These cells are critical for ensuring normal neuronal function through glutamate uptake, maintaining homeostasis of the extracellular environment, water transport, and preserving the integrity of the blood-brain barrier (BBB). As the third member of the tripartite synapse, astrocytes are capable of modulating neural communication via the release of gliotransmitters (adenosine triphosphate (ATP), glutamate, and D-serine)(Salatino et al. 2017a). Upon activation, astrocytes enter a reactive state. This reactive state is characterized by an upregulation of glial fibrillary acidic

protein (GFAP), cellular hypertrophy, and proliferation(He and Bellamkonda 2008; Campbell et al. 2018). Microglia are the resident macrophages in the brain. In a resting state, microglia monitor the environment with their many long, thin processes. Insertion of the MEA activates microglia, causing them to take on a more compact shape, proliferate, and migrate towards the injury(Perry and Teeling 2013). Together, activated astrocytes and microglia form an encapsulating sheath around the MEA, creating a physical barrier and isolating neurons from the electrode.

Blood brain barrier rupture

The cortex has the highest density of blood vessels in the brain, as many as 160 capillaries per mm^2, with vessels forming an intricate and compact network(Cavaglia et al. 2001). As the MEA is inserted, capillaries are severed, pulled, and ruptured, resulting in the disruption of the (BBB) and the leakage of blood into the central nervous system (CNS). Hemoglobin is released as blood cells break down, increasing the level of reactive oxygen species (ROS). Oxidative stress leads to further BBB rupture via downregulation of tight junction proteins and oxidation of cell membranes(He and Bellamkonda 2008; Kozai et al. 2015b).

Blood serum proteins such as albumin, thrombin, and fibrinogen are released into the CNS due to BBB rupture, initiating a signaling cascade that can cause further damage. Albumin binds to transforming growth factor-β (TGF-β) receptors on astrocytes, resulting in an upregulation of myosin light chain kinase (MLCK). Subsequently, MLCK phosphorylates myosin light chain (MLC), inducing contractions and weakening endothelial cell-cell adhesion causing further BBB leakage(Shen et al. 2010; Rossi et al. 2011). In addition, albumin activates astrocytes and microglia via the mitogen-activated protein kinase (MAPK) pathway resulting in an increase in interleukin-1 beta (IL-1β), an inflammatory cytokine, and nitric oxide(Ralay Ranaivo and Wainwright 2010).

Thrombin contributes to the foreign body response through several pathways. As a component of the coagulation cascade, thrombin polymerizes fibrinogen into fibrin; a process that has been

linked to demyelination in multiple sclerosis. Thrombin also acts as an activator of astrocytes and microglia via activation of proteinase-activated receptors (PAR)(He and Bellamkonda 2008). In astrocytes, activation of PAR-1 induces a sustained activation of extracellular receptor kinase (ERK) via recruitment of the MAPK pathway through G coupled protein receptors, resulting in an increase of cyclin D1 and ultimately astrocyte proliferation, morphological changes, and secretion of endothelin-1. In microglia, thrombin activation of PAR-1 induces microglial activation, as evidenced by increased proliferation and nitric oxide (NO) production(Weinstein et al. 1995; He and Bellamkonda 2008). Although some mild cytokine release is associated with PAR-1 activation, activation of PAR-4 is paramount for cytokine production. Thrombin activation of PAR-4 leads to a prolonged increase in calcium followed by MAPK3 activation and subsequent nuclear factor κB (NF-κB) activation, ultimately inducing cytokine production(Suo et al. 2003; He and Bellamkonda 2008).

Molecular mediators of the reactive response

Reactive microglia and astrocytes release pro-inflammatory cytokines including tumor necrosis factor α (TNF-α), TGF-β, and interleukins 1 and 6 (IL-1 and IL-6). Cytokines act as mediators of intercellular communication for the initiation and propagation of the reactive immune response(Polikov et al. 2005; Buffo et al. 2010; Campbell et al. 2018). TNF-α maintains the activated status of microglia via the autocrine loop and induces proliferation in astrocytes. In addition, TNF-α has been shown to have direct cytoxic effects on oligodendrocytes and neurons(Downen et al. 1999; Chen and Swanson 2003). IL-1 exists in both a membrane bound (IL-1α) and secreted form (IL-1β). IL-1β has particularly strong effects on astrocytes, promoting and modulating astrogliosis through upregulation of GFAP expression, increasing proliferation and the production of cytokines, matrix proteins and growth factors. In microglia, IL-1β can amplify the inflammation signal via an autocrine feedback loop, leading to further stimulation of activation. IL-6 has similar pro-inflammatory effects on astrocytes, however, unlike IL-1, IL-6 can also act in an anti-inflammatory matter. IL-6 shares signaling receptors with multiple growth

factors. Activation of these receptors can lead to the promotion of neurite growth, neuronal survival, and downregulation of TNF-α(He and Bellamkonda 2008; Kozai et al. 2015b; Campbell et al. 2018). Similarly, TGF-β exhibits both pro- and anti-inflammatory effects. TGF-β acts an anti-inflammatory cytokine by inhibiting gial cell proliferation and the expression of TNF-α and IL-1, however, when highly expressed, TGF-β exacerbates reactive astrogliosis and glial scar formation(Campbell et al. 2018).

Heterogeneity of reactive astrocytes

Reactive astrogliosis, however, is not a singular uniform response but a context dependent reaction that results in variations on multiple levels. Reactive astrocytes take on a variety of forms and functions depending on the nature of the injury and the surrounding environment, and are capable of having either neurotoxic or neuroprotective effects. Although hypertrophy is a common morphological feature of reactive astrocytes, the degree of hypertrophy depends on proximity and severity of the injury. Additionally, astrocyte processes typically do not overlap in uninjured tissue and moderate reactive astrogliosis; however, during severe astrogliosis, where proliferation is present, astrocytic processes often intertwine(Anderson et al. 2014). Moreover, gene up- and downregulation are dependent on both injury type and mediators of astrocyte activation(Zamanian et al. 2012; Anderson et al. 2014). This heterogeneity suggests possible reactive astrocyte subtypes; however, the relationship between the different geno- and phenotypes of reactive astrocytes and various insults has not been fully explored. Ultimately, the reactive immune response results in the encapsulation of the MEA by glial cells, the loss of neurons at the neural-electrode interface, and device failure.

Summary

In this thesis I explore the heterogeneity of astrogliosis and methods of perturbing the reactive immune response. Chapter one is taken from an article published in IEEE(Winter et al. 2017) and explores means of perturbing the reactive immune response by altering the tissue composition at the neural-electrode interface. I was the first author of this manuscript, which

included experimental data from multiple projects and lab members*. My contribution to the research specifically focused on the use of transcription factors to reprogram astrocytes. Rat cortical astrocytes were cultured *in vitro* and subsequently infected with transcription factors *Ascl1*, *Dlx2*, or both to reprogram astrocytes into functional neurons. Electrophysiological recordings and anti-beta 3 tubulin staining were performed 5 to 21 days post-infection to determine neuronal identity. Cells infected with both transcription factors achieved a neuronal morphology at earlier time points than those infected with either transcription factor alone. While single spike activity was observed under all conditions, electrical properties were inconsistent and did not exhibit a trend of cells acquiring mature firing characteristics.

Chapter two is taken from a first-author publication in Micromachines(Winter et al. 2018) and describes methods of delivering viral vectors *in vivo* to alter gene expression at the neural-microelectrode interface in chronic settings*. Microfluidic MEAs were implanted in the motor cortex of rats. One to three weeks post-implantation viral vectors were delivered to upregulate, knockdown, or conditionally express genes. Two weeks post-infusion, rats were sacrificed, brains were explanted and cryosectioned to verify vector delivery. Data show that viral vectors were successfully delivered along the entire length of the injury, however, due to the geometry of the device the virus was more highly expressed and dispersed at deeper sections of injury compared to superficial regions. These results indicate that microfluidic devices are viable tools to perturb and mediate the reactive immune response *in vivo*.

Chapter three focuses on future directions for the work, which includes the identification of unique reactive astrocyte subtypes induced by MEA implantation. Rat cortical astrocytes were cultured in serum free media. Subsequently, cells were exposed to either a combination of cytokines (TNF-α, IL-1β, complement component 1 subcomponent q (C1q)), γ-aminobutyric acid (GABA), or both for 24 hours. Cells were fixed and stained for GFAP and complement component 3 subcomponent d (C3d) to identify reactive astrocytes and the neurotoxic “A1”

reactive astrocyte subtype respectively(Liddelow et al. 2017). GFAP expression was not significantly altered by neither cytokine nor GABA exposure; however, GABA exposure resulted in significantly elevated C3d expression. These preliminary results suggest that electrode implantation could induce neurotoxic reactive astrocytes, however, further research is required to fully characterize these observations.

BIBLIOGRAPHY

BIBLIOGRAPHY

Adelman G, **Rane SG**, **Villa KF**. The cost burden of multiple sclerosis in the United States: a systematic review of the literature. *J Med Econ* 16: 639–647, 2013.

Anderson MA, **Ao Y**, **Sofroniew M V.** Heterogeneity of reactive astrocytes. *Neurosci Lett* 565: 23–29, 2014.

Anikeeva P, **Andalman AS**, **Witten I**, **Warden M**, **Goshen I**, **Grosenick L**, **Gunaydin LA**, **Frank LM**, **Deisseroth K**. Optetrode: a multichannel readout for optogenetic control in freely moving mice. *Nat Neurosci* 15: 163–70, 2011.

Arthur KC, **Calvo A**, **Price TR**, **Geiger JT**, **Chiò A**, **Traynor BJ**. Projected increase in amyotrophic lateral sclerosis from 2015 to 2040. *Nat Commun* 7: 12408, 2016.

Bedell HW, **Hermann JK**, **Ravikumar M**, **Lin S**, **Rein A**, **Li X**, **Molinich E**, **Smith PD**, **Selkirk SM**, **Miller RH**, **Sidik S**, **Taylor DM**, **Capadona JR**. Targeting CD14 on blood derived cells improves intracortical microelectrode performance. *Biomaterials* 163: 163–173, 2018.

Benabid AL, **Chabardes S**, **Torres N**, **Piallat B**, **Krack P**, **Fraix V**, **Pollak P**. Functional neurosurgery for movement disorders: a historical perspective. *Prog. Brain Res.* 175: 379–391, 2009.

Bennett C, **Samikkannu M**, **Mohammed F**, **Dietrich WD**, **Rajguru SM**, **Prasad A**. Blood brain barrier (BBB)-disruption in intracortical silicon microelectrode implants. *Biomaterials* 164: 1–10, 2018.

Biran R, **Martin DC**, **Tresco PA**. Neuronal cell loss accompanies the brain tissue response to chronically implanted silicon microelectrode arrays. *Exp Neurol* 195: 115–126, 2005.

Bouton CE, **Shaikhouni A**, **Annetta N V.**, **Bockbrader MA**, **Friedenberg DA**, **Nielson DM**, **Sharma G**, **Sederberg PB**, **Glenn BC**, **Mysiw WJ**, **Morgan AG**, **Deogaonkar M**, **Rezai AR**. Restoring cortical control of functional movement in a human with quadriplegia. *Nature* 533: 247–250, 2016.

Buffo A, **Rolando C**, **Ceruti S**. Astrocytes in the damaged brain: Molecular and cellular insights into their reactive response and healing potential. *Biochem Pharmacol* 79: 77–89, 2010.

Campbell A, **Wu C**, **Campbell A**, **Wu C**. Chronically Implanted Intracranial Electrodes: Tissue Reaction and Electrical Changes. *Micromachines* 9: 430, 2018.

Canales A, **Jia X**, **Froriep UP**, **Koppes RA**, **Tringides CM**, **Selvidge J**, **Lu C**, **Hou C**, **Wei L**, **Fink Y**, **Anikeeva P**. Multifunctional fibers for simultaneous optical, electrical and chemical interrogation of neural circuits in vivo. *Nat Biotechnol* 33: 277–284, 2015.

Cardin JA, **Carlén M**, **Meletis K**, **Knoblich U**, **Zhang F**, **Deisseroth K**, **Tsai L-H**, **Moore CI**. Targeted optogenetic stimulation and recording of neurons in vivo using cell-type-specific expression of Channelrhodopsin-2. *Nat Protoc* 5: 247–254, 2010.

Cavaglia M, **Dombrowski SM**, **Drazba J**, **Vasanji A**, **Bokesch PM**, **Janigro D**. Regional variation in brain capillary density and vascular response to ischemia. *Brain Res* 910: 81–93, 2001.

Chen R, **Canales A**, **Anikeeva P**. Neural recording and modulation technologies. *Nat Rev Mater* 2: 16093, 2017.

Chen Y, **Swanson RA**. Astrocytes and Brain Injury. *J Cereb Blood Flow Metab* 23: 137–149, 2003.

Chen Z-J, **Gillies GT**, **Broaddus WC**, **Prabhu SS**, **Fillmore H**, **Mitchell RM**, **Corwin FD**, **Fatouros PP**. A realistic brain tissue phantom for intraparenchymal infusion studies. *J Neurosurg* 101: 314–322, 2004.

Collinger JL, **Wodlinger B**, **Downey JE**, **Wang W**, **Tyler-Kabara EC**, **Weber DJ**, **McMorland AJ**, **Velliste M**, **Boninger ML**, **Schwartz AB**. High-performance neuroprosthetic control by an individual with tetraplegia. *Lancet* 381: 557–564, 2013.

Dorsey ER, **Constantinescu R**, **Thompson JP**, **Biglan KM**, **Holloway RG**, **Kieburtz K**, **Marshall FJ**, **Ravina BM**, **Schifitto G**, **Siderowf A**, **Tanner CM**. Projected number of people with Parkinson disease in the most populous nations, 2005 through 2030. *Neurology* 68: 384–386, 2007.

Downen M, **Amaral TD**, **Hua LL**, **Zhao M-L**, **Lee SC**. Neuronal death in cytokine-activated primary human brain cell culture: role of tumor necrosis factor-? *Glia* 28: 114–127, 1999.

Eles JR, **Vazquez AL**, **Kozai TDY**, **Cui XT**. In vivo imaging of neuronal calcium during electrode implantation: Spatial and temporal mapping of damage and recovery. *Biomaterials* 174: 79–94, 2018.

Ereifej ES, **Smith CS**, **Meade SM**, **Chen K**, **Feng H**, **Capadona JR**. The Neuroinflammatory Response to Nanopatterning Parallel Grooves into the Surface Structure of Intracortical Microelectrodes. *Adv Funct Mater* 28: 1704420, 2018.

Ezzyat Y, **Wanda PA**, **Levy DF**, **Kadel A**, **Aka A**, **Pedisich I**, **Sperling MR**, **Sharan AD**, **Lega BC**, **Burks A**, **Gross RE**, **Inman CS**, **Jobst BC**, **Gorenstein MA**, **Davis KA**, **Worrell GA**, **Kucewicz MT**, **Stein JM**, **Gorniak R**, **Das SR**, **Rizzuto DS**, **Kahana MJ**. Closed-loop stimulation of temporal cortex rescues functional networks and improves memory. *Nat Commun* 9: 365, 2018.

Golabchi A, **Wu B**, **Li X**, **Carlisle DL**, **Kozai TDY**, **Friedlander RM**, **Cui XT**. Melatonin improves quality and longevity of chronic neural recording. *Biomaterials* 180: 225–239, 2018.

Greenberg PE, **Kessler RC**, **Birnbaum HG**, **Leong SA**, **Lowe SW**, **Berglund PAA**, **Corey-Lisle PK**. The Economic Burden of Depression in the United States: How Did It Change Between 1990 and 2000? *J Clin Psychiatry* 64: 1465–1475, 2003.

Guo Z, **Zhang L**, **Wu Z**, **Chen Y**, **Wang F**, **Chen G**. In Vivo Direct Reprogramming of Reactive Glial Cells into Functional Neurons after Brain Injury and in an Alzheimer's Disease Model. *Cell Stem Cell* 14: 188–202, 2014.

Halpern CH, **Samadani U**, **Litt B**, **Jaggi JL**, **Baltuch GH**. Deep Brain Stimulation for Epilepsy. In: *Neuromodulation*. Elsevier, p. 639–649.

Hascup KN, **Hascup ER**, **Stephens ML**, **Glaser PEA**, **Yoshitake T**, **Mathé AA**, **Gerhardt GA**, **Kehr J**. Resting glutamate levels and rapid glutamate transients in the prefrontal cortex of the Flinders Sensitive Line rat: a genetic rodent model of depression. *Neuropsychopharmacology* 36: 1769–77, 2011.

He W, **Bellamkonda R V.** A Molecular Perspective on Understanding and Modulating the Performance of Chronic Central Nervous System (CNS) Recording Electrodes [Online]. CRC Press/Taylor & Francis. http://www.ncbi.nlm.nih.gov/pubmed/21204400 [31 Oct. 2018].

Heinrich C, **Blum R**, **Gascón S**, **Masserdotti G**, **Tripathi P**, **Sánchez R**, **Tiedt S**, **Schroeder T**, **Götz M**, **Berninger B**. Directing Astroglia from the Cerebral Cortex into Subtype Specific Functional Neurons. *PLoS Biol* 8: e1000373, 2010.

Igarashi H, **Koizumi K**, **Kaneko R**, **Ikeda K**, **Egawa R**, **Yanagawa Y**, **Muramatsu S**, **Onimaru H**, **Ishizuka T**, **Yawo H**. A Novel Reporter Rat Strain That Conditionally Expresses the Bright Red Fluorescent Protein tdTomato. *PLoS One* 11: e0155687, 2016.

Jennings JH, **Stuber GD**. Tools for Resolving Functional Activity and Connectivity within Intact Neural Circuits. *Curr Biol* 24: R41–R50, 2014.

Jeong J-W, **McCall JG**, **Shin G**, **Zhang Y**, **Al-Hasani R**, **Kim M**, **Li S**, **Sim JY**, **Jang K-I**, **Shi Y**, **Hong DY**, **Liu Y**, **Schmitz GP**, **Xia L**, **He Z**, **Gamble P**, **Ray WZ**, **Huang Y**, **Bruchas MR**, **Rogers JA**. Wireless Optofluidic Systems for Programmable In Vivo Pharmacology and Optogenetics. *Cell* 162: 662–674, 2015.

Jorfi M, **Skousen JL**, **Weder C**, **Capadona JR**. Progress towards biocompatible intracortical microelectrodes for neural interfacing applications. *J Neural Eng* 12: 011001, 2015.

Karumbaiah L, **Saxena T**, **Carlson D**, **Patil K**, **Patkar R**, **Gaupp EA**, **Betancur M**, **Stanley GB**, **Carin L**, **Bellamkonda R V.** Relationship between intracortical electrode design and chronic recording function. *Biomaterials* 34: 8061–8074, 2013.

Khan W, **Li W**. Wafer level fabrication method of hemispherical reflector coupled micro-led array stimulator for optogenetics. In: *2017 19th International Conference on Solid-State Sensors, Actuators and Microsystems (TRANSDUCERS)*. IEEE, p. 2231–2234.

Konermann S, **Brigham MD**, **Trevino A**, **Hsu PD**, **Heidenreich M**, **Cong L**, **Platt RJ**, **Scott DA**, **Church GM**, **Zhang F**. Optical control of mammalian endogenous transcription and epigenetic states. *Nature* 500: 472–476, 2013.

Kowal SL, **Dall TM**, **Chakrabarti R**, **Storm M V.**, **Jain A**. The current and projected economic burden of Parkinson's disease in the United States. *Mov Disord* 28: 311–318, 2013.

Kozai TDY, **Catt K**, **Li X**, **Gugel Z V.**, **Olafsson VT**, **Vazquez AL**, **Cui XT**. Mechanical failure modes of chronically implanted planar silicon-based neural probes for laminar recording. *Biomaterials* 37: 25–39, 2015a.

Kozai TDY, **Gugel Z**, **Li X**, **Gilgunn PJ**, **Khilwani R**, **Ozdoganlar OB**, **Fedder GK**, **Weber DJ**,

Cui XT. Chronic tissue response to carboxymethyl cellulose based dissolvable insertion needle for ultra-small neural probes. *Biomaterials* 35: 9255–9268, 2014.

Kozai TDY, **Jaquins-Gerstl AS**, **Vazquez AL**, **Michael AC**, **Cui XT**. Brain tissue responses to neural implants impact signal sensitivity and intervention strategies. *ACS Chem Neurosci* 6: 48–67, 2015b.

Kozai TDY, **Jaquins-Gerstl AS**, **Vazquez AL**, **Michael AC**, **Cui XT**. Dexamethasone retrodialysis attenuates microglial response to implanted probes in vivo. *Biomaterials* 87: 157–169, 2016.

Kozai TDY, **Langhals NB**, **Patel PR**, **Deng X**, **Zhang H**, **Smith KL**, **Lahann J**, **Kotov NA**, **Kipke DR**. Ultrasmall implantable composite microelectrodes with bioactive surfaces for chronic neural interfaces. *Nat Mater* 11: 1065–1073, 2012.

Lebedev MA, **Nicolelis MAL**. Brain–machine interfaces: past, present and future. *Trends Neurosci* 29: 536–546, 2006.

Lee M, **Schwab C**, **Mcgeer PL**. Astrocytes are GABAergic cells that modulate microglial activity. *Glia* 59: 152–165, 2011.

Liddelow SA, **Guttenplan KA**, **Clarke LE**, **Bennett FC**, **Bohlen CJ**, **Schirmer L**, **Bennett ML**, **Münch AE**, **Chung W-S**, **Peterson TC**, **Wilton DK**, **Frouin A**, **Napier BA**, **Panicker N**, **Kumar M**, **Buckwalter MS**, **Rowitch DH**, **Dawson VL**, **Dawson TM**, **Stevens B**, **Barres BA**. Neurotoxic reactive astrocytes are induced by activated microglia. *Nature* 541: 481–487, 2017.

Ludwig K a, **Uram JD**, **Yang J**, **Martin DC**, **Kipke DR**. Chronic neural recordings using silicon microelectrode arrays electrochemically deposited with a poly(3,4-ethylenedioxythiophene) (PEDOT) film. *J Neural Eng* 3: 59–70, 2006.

Ludwig KA, **Miriani RM**, **Langhals NB**, **Joseph MD**, **Anderson DJ**, **Kipke DR**. Using a Common Average Reference to Improve Cortical Neuron Recordings From Microelectrode Arrays. *J Neurophysiol* 101: 1679–1689, 2009.

Malaga KA, **Schroeder KE**, **Patel PR**, **Irwin ZT**, **Thompson DE**, **Bentley JN**, **Lempka SF**, **Chestek CA**, **Patil PG**. Data-driven model comparing the effects of glial scarring and interface interactions on chronic neural recordings in non-human primates. *J Neural Eng J Neural Eng* 13: 16010–16024, 2016.

Malone DA, **Dougherty DD**, **Rezai AR**, **Carpenter LL**, **Friehs GM**, **Eskandar EN**, **Rauch SL**, **Rasmussen SA**, **Machado AG**, **Kubu CS**, **Tyrka AR**, **Price LH**, **Stypulkowski PH**, **Giftakis JE**, **Rise MT**, **Malloy PF**, **Salloway SP**, **Greenberg BD**. Deep Brain Stimulation of the Ventral Capsule/Ventral Striatum for Treatment-Resistant Depression. *Biol Psychiatry* 65: 267–275, 2009.

Mayberg HS, **Lozano AM**, **Voon V**, **McNeely HE**, **Seminowicz D**, **Hamani C**, **Schwalb JM**, **Kennedy SH**. Deep Brain Stimulation for Treatment-Resistant Depression. *Neuron* 45: 651–660, 2005.

McCreery D, **Cogan S**, **Kane S**, **Pikov V**. Correlations between histology and neuronal activity recorded by microelectrodes implanted chronically in the cerebral cortex. *J Neural Eng* 13:

036012, 2016.

Michelson NJ, **Vazquez AL**, **Eles JR**, **Salatino JW**, **Purcell EK**, **Williams JJ**, **Cui XT**, **Kozai TDY**. Multi-scale, multi-modal analysis uncovers complex relationship at the brain tissue-implant neural interface: new emphasis on the biological interface. *J Neural Eng* 15: 033001, 2018.

Motta-Mena LB, **Reade A**, **Mallory MJ**, **Glantz S**, **Weiner OD**, **Lynch KW**, **Gardner KH**. An optogenetic gene expression system with rapid activation and deactivation kinetics. *Nat Chem Biol* 10: 196–202, 2014.

Nagy A. Cre recombinase: The universal reagent for genome tailoring. *genesis* 26: 99–109, 2000.

Nolta NF, **Christensen MB**, **Crane PD**, **Skousen JL**, **Tresco PA**. BBB leakage, astrogliosis, and tissue loss correlate with silicon microelectrode array recording performance. *Biomaterials* 53: 753–762, 2015.

O'Doherty JE, **Lebedev MA**, **Ifft PJ**, **Zhuang KZ**, **Shokur S**, **Bleuler H**, **Nicolelis MAL**. Active tactile exploration using a brain-machine-brain interface. *Nature* 479: 228–31, 2011.

Oakes RS, **Polei MD**, **Skousen JL**, **Tresco PA**. An astrocyte derived extracellular matrix coating reduces astrogliosis surrounding chronically implanted microelectrode arrays in rat cortex. *Biomaterials* 154: 1–11, 2018.

Perry VH, **Teeling J**. Microglia and macrophages of the central nervous system: the contribution of microglia priming and systemic inflammation to chronic neurodegeneration. *Semin Immunopathol* 35: 601–12, 2013.

Polikov VS, **Tresco PA**, **Reichert WM**. Response of brain tissue to chronically implanted neural electrodes. *J Neurosci Methods* 148: 1–18, 2005.

Potter KA, **Buck AC**, **Self WK**, **Callanan ME**, **Sunil S**, **Capadona JR**. The effect of resveratrol on neurodegeneration and blood brain barrier stability surrounding intracortical microelectrodes. *Biomaterials* 34: 7001–7015, 2013.

Purcell EK, **Thompson DE**, **Ludwig KA**, **Kipke DR**. Flavopiridol reduces the impedance of neural prostheses in vivo without affecting recording quality. *J Neurosci Methods* 183: 149–157, 2009.

Purcell EK, **Yang A**, **Liu L**, **Velkey JM**, **Morales MM**, **Duncan RK**. BDNF profoundly and specifically increases KCNQ4 expression in neurons derived from embryonic stem cells. *Stem Cell Res* 10: 29–35, 2013.

Ralay Ranaivo H, **Wainwright MS**. Albumin activates astrocytes and microglia through mitogen-activated protein kinase pathways. *Brain Res* 1313: 222–31, 2010.

Rennaker RL, **Miller J**, **Tang H**, **Wilson DA**. Minocycline increases quality and longevity of chronic neural recordings. *J Neural Eng* 4: L1-5, 2007.

Rosin B, **Slovik M**, **Mitelman R**, **Rivlin-Etzion M**, **Haber SN**, **Israel Z**, **Vaadia E**, **Bergman H**. Closed-Loop Deep Brain Stimulation Is Superior in Ameliorating Parkinsonism. *Neuron* 72: 370–

384, 2011.

Rossi JL, **Ralay Ranaivo H**, **Patel F**, **Chrzaszcz M**, **Venkatesan C**, **Wainwright MS**. Albumin causes increased myosin light chain kinase expression in astrocytes via p38 mitogen-activated protein kinase. *J Neurosci Res* 89: 852–61, 2011.

Salatino JW, **Ludwig KA**, **Kozai TDY**, **Purcell EK**. Glial responses to implanted electrodes in the brain. *Nat Biomed Eng* 1: 862–877, 2017a.

Salatino JW, **Winter BM**, **Drazin MH**, **Purcell EK**. Functional remodeling of subtype-specific markers surrounding implanted neuroprostheses. *J Neurophysiol* 118: 194–202, 2017b.

Seidl K, **Spieth S**, **Herwik S**, **Steigert J**, **Zengerle R**, **Paul O**, **Ruther P**. In-plane silicon probes for simultaneous neural recording and drug delivery. *J Micromechanics Microengineering* 20: 105006, 2010.

Seymour JP, **Kipke DR**. Neural probe design for reduced tissue encapsulation in CNS. *Biomaterials* 28: 3594–3607, 2007.

Shen Q, **Rigor RR**, **Pivetti CD**, **Wu MH**, **Yuan SY**. Myosin light chain kinase in microvascular endothelial barrier function. *Cardiovasc Res* 87: 272–80, 2010.

Shen W, **Karumbaiah L**, **Liu X**, **Saxena T**, **Chen S**, **Patkar R**, **Bellamkonda R V.**, **Allen MG**. Extracellular matrix-based intracortical microelectrodes: Toward a microfabricated neural interface based on natural materials. *Microsystems Nanoeng* 1: 15010, 2015.

Sofroniew M V. Molecular dissection of reactive astrogliosis and glial scar formation. *Trends Neurosci* 32: 638–47, 2009.

Sofroniew M V. Astrogliosis. *Cold Spring Harb Perspect Biol* 7: a020420, 2014.

Sofroniew M V, **Vinters H V**. Astrocytes: biology and pathology. *Acta Neuropathol* 119: 7–35, 2010.

Sommakia S, **Lee HC**, **Gaire J**, **Otto KJ**. Materials approaches for modulating neural tissue responses to implanted microelectrodes through mechanical and biochemical means. *Curr Opin Solid State Mater Sci* 18: 319–328, 2014.

Suo Z, **Wu M**, **Citron BA**, **Gao C**, **Festoff BW**. Persistent protease-activated receptor 4 signaling mediates thrombin-induced microglial activation. *J Biol Chem* 278: 31177–83, 2003.

Tong M, **Hernandez JL**, **Purcell EK**, **Altschuler RA**, **Duncan RK**. The intrinsic electrophysiological properties of neurons derived from mouse embryonic stem cells overexpressing neurogenin-1. *Am J Physiol Physiol* 299: C1335–C1344, 2010.

Vierbuchen T, **Ostermeier A**, **Pang ZP**, **Kokubu Y**, **Südhof TC**, **Wernig M**. Direct conversion of fibroblasts to functional neurons by defined factors. *Nature* 463: 1035–1041, 2010.

Volterra A, **Meldolesi J**. Astrocytes, from brain glue to communication elements: the revolution continues. *Nat Rev Neurosci* 6: 626–640, 2005.

Weaver FM, **Follett K**, **Stern M**, **Hur K**, **Harris C**, **Marks WJ**, **Rothlind J**, **Sagher O**, **Reda D**, **Moy CS**, **Pahwa R**, **Burchiel K**, **Hogarth P**, **Lai EC**, **Duda JE**, **Holloway K**, **Samii A**, **Horn S**, **Bronstein J**, **Stoner G**, **Heemskerk J**, **Huang GD**, **Group for the C 468 S**, **KA F**, **S M**, **J C**, **RL R**, **F W**, **AE L**, **Y T**, **P K**, **G D**, **MM H**, **JW L**, **MF F**, **S F**, **RS S**, **V P**, **RA H**, **CG G**, **R P**, **A S**, **K S-T**, **H J**, **P L**, **K W**, **M A**, **BS A**, **Y T**, **KJ B**, **MI H**. Bilateral Deep Brain Stimulation vs Best Medical Therapy for Patients With Advanced Parkinson Disease<subtitle>A Randomized Controlled Trial</subtitle> *JAMA* 301: 63, 2009.

Weinstein JR, **Gold SJ**, **Cunningham DD**, **Gall CM**, **Sastre A**, **Lyuboslavsky P**, **Hepler JR**, **McKeon RJ**, **Traynelis SF**. Cellular localization of thrombin receptor mRNA in rat brain: expression by mesencephalic dopaminergic neurons and codistribution with prothrombin mRNA. *J Neurosci* 15: 2906–19, 1995.

Wellman SM, **Eles JR**, **Ludwig KA**, **Seymour JP**, **Michelson NJ**, **McFadden WE**, **Vazquez AL**, **Kozai TDY**. A Materials Roadmap to Functional Neural Interface Design. *Adv Funct Mater* 28: 1701269, 2018.

Wimo A, **Jönsson L**, **Bond J**, **Prince M**, **Winblad B**, **Alzheimer Disease International**. The worldwide economic impact of dementia 2010. *Alzheimers Dement* 9: 1–11.e3, 2013.

Winter B, **Daniels S**, **Salatino J**, **Purcell E**. Genetic Modulation at the Neural Microelectrode Interface: Methods and Applications. *Micromachines 2018, Vol 9, Page 476* 9: 476, 2018.

Winter BM, **Setien MB**, **Salatino JW**, **Blanke N**, **Thompson CH**, **Smith KR**, **Khan WA**, **Li W**, **Suhr ST**, **Purcell EK**. Control of cell fate and excitability at the neural electrode interface: Genetic reprogramming and optical induction. In: *2017 IEEE Life Sciences Conference (LSC)*. IEEE, p. 157–161.

Zamanian JL, **Xu L**, **Foo LC**, **Nouri N**, **Zhou L**, **Giffard RG**, **Barres BA**. Genomic analysis of reactive astrogliosis. *J Neurosci* 32: 6391–410, 2012.

CHAPTER 1 Control of Cell Fate and Excitability at the Neural Electrode Interface: Genetic Reprogramming and Optical Induction

Introduction

Microelectrode arrays (MEAs) implanted in the brain have shown increasing potential to both understand and treat neurological injuries and diseases. One of the most notable clinical successes is the use of deep brain stimulation to alleviate the dyskinesia and akinesia symptoms of Parkinson's disease (Benabid et al. 2009). Additionally, implanted MEAs have been used to read out information from the brain, enabling control of prostheses and restoring upper limb function in quadriplegic patients (Collinger et al. 2013; Bouton et al. 2016). The long term efficacy of these technologies, however, is impeded by the reactive tissue response to the implanted device. Implantation of an electrode causes an encapsulating cellular sheath to form, wherein a layer of microglia reside at the electrode interface surrounded by a larger region of astroglial reactivity (Biran et al. 2005). Temporal and spatial variations exist within this sheath that contribute to the isolation of the electrode from neurons over time. These effects are believed to contribute to shifting stimulation thresholds, instability, and recording loss over time.

To both understand and control the reactive tissue response to brain implants, we are developing new approaches to genetically reprogram the identity of cells at the implanted electrode interface. Previous studies have shown that glutamatergic neurons can be generated from astroglia via the overexpression of Neurogenin-2 (Heinrich et al. 2010) or NeuroD1 (Guo et al. 2014), while combined delivery of Ascl1 and Dlx2 can produce GABAergic neurons (Heinrich et al. 2010). Further, based on recent reports (Konermann et al. 2013; Motta-Mena et al. 2014), we are pursuing methods to control the expression of these proneural genes in response to optical stimulation. For this, we are coupling proneural gene expression to a recently described bacterial transcription factor that enables blue light-dependent transcriptional activation ("EL222")(Motta-Mena et al. 2014). Optical stimulation allows for precise spatiotemporal control

of gene induction and may be accomplished via device-integrated microLED arrays *in vivo*(Khan and Li 2017). These successes imply that not only can the glial sheath be converted into functional neurons, but that the heterogeneity of the native tissue can be restored in prescribed spatiotemporal patterns at the tissue-device interface.

Methods

Expression vectors

Constitutive expression vectors. Retroviral expression vectors containing a strong constitutive promoter (CMV immediate-early or LTR) were used either as vectors for production of recombinant, replication-defective retroviral particles or as expression plasmids for testing by transient transfection of HEK293 cells. Genes were expressed from constitutive vectors for two reasons: 1) To provide the transactivator needed for light-responsive gene expression, or 2) To assess the pro-neural capacity of individual factors on different target cells for eventual use in the light-inducible system.

For constitutive expression of the light-responsive transactivator, a synthetic DNA encoding a nuclear localization signal (NLS), a strong transactivation domain (VP16), and the light-responsive DNA-binding protein EL222 (NVE) was utilized.

For constitutive expression of pro-neural genes for testing on target cell types (astrocytes and CNS progenitors), the open-reading-frames (ORFs) of five transcription factors demonstrated in human, mouse or rat cells to promote neural identity or maturation were produced by PCR amplification of genomic DNA, brain cDNA, or synthetic DNA. ORFs for the factors ASCL1, Pou3F2, NeuroD1, Neurogenin-2 and Dlx-2 were isolated and inserted in-frame with YFP to allow real-time monitoring of expression and localization of the expressed proteins.

Light-responsive expression vectors. For the reporter vectors, six tandem EL222 responsive elements (ELREs) coupled to a minimal CMV promoter were introduced into retroviral vector plasmids immediately upstream of reporter genes including eYFP, dsREDexp, and firefly luciferase or the pro-neural factors described above. Preliminary results (not shown) indicated

that this design produced reporter vectors with minimal basal activity and maximal response to light-activated NVE.

Virus production. Recombinant replication-defective virus was packaged by 3-way transfection of the individual vector plasmids and with gag-pol and VSVg-encoding packaging plasmids in HEK293 cells using standard methods. In brief, 48-hours post transfection, viral supernatants were harvested and subject to low-speed centrifugation to remove bulk cells, filtered through a 0.45um filter to remove any remaining cells and fine debris, and then concentrated by high-speed centrifugation. The pellet of concentrated virus was then resuspended in 75-100ul of PBS and frozen in aliquots at -80^{o}C until use.

Cell culture and transfection/infection

Three cell types were cultured for use in experiments: 1) HEK293 cells, 2) Rat primary cortical astrocytes, and 3) CNS progenitor cells derived from rat induced pluripotent stem cells (iPSCs).

HEK cells. HEK293 cells were used for viral packaging (see above) and for preliminary testing of the light-responsive activator and reporter vectors. HEKs were grown in Dulbecco's modified Eagle's medium (DMEM; Life Technologies) supplemented with 10% FBS (Sigma), and 1% penicillin/streptomycin (Life Technologies) in a 5% CO2 incubator. HEKs were cultured in 15-cm plates for virus production or 12/24-well plates for transient transfection assays. Transfection was performed by standard methods using calcium phosphate co-precipitation of plasmid DNAs within 24-hours of passage followed by a change of medium 18-24-hours post-transfection.

Astrocytes. Rat primary cortical astrocytes were seeded and maintained according to manufacturer specifications (Fisher Scientific Company) in HEK medium supplemented with 20% FBS in 6-well plates (Sigma). For infection with recombinant viruses, 5-20ul of concentrated viral stock was added to individual wells of astrocytes at approx. 90% confluency and allowed to incubate overnight undisturbed. The next day, the astrocyte medium was exchanged for neuronal culture medium (1mL B27, 125 uLGlutaMax in 50mL Neurobasal Media) and cultured in a 5% CO2 incubator with medium changes every 2-3 days until analysis.

CNS progenitors. Neural progenitor cells (NPCs) derived from rat induced pluripotent stem cells (iPSCs) were initially expanded in 6-well plates (Sigma) coated with fibronectin (8µg/ml in PBS; Thermo Fisher) in defined medium (DMEM/F12 with 10% N-2 supplement, 1% penicillin/streptomycin and 25 ng/ml rat EGF (endothelial growth factor) and FGF-2 (basic fibroblast growth factor)) in a 5% CO2 incubator. NPCs at passage 2-4 were seeded in 24-well plates with polyornithine-laminin coating (10 µg/ml in dH_2O) and infected with virus essentially as described above for astrocytes. The medium of infected NPCs was changed 16-24 hours later and the cell were exposed to light and examined as described below.

Whole cell electrophysiology

To assess the success of neuronal conversion, we performed whole cell electrophysiology to identify spiking activity in response to injected current. Cells were placed in carboxygenated physiological extracellular solution (in mM: 126 NaCl, 2.5 KCl, 1.25 NaH2PO4, 2 CaCl22H20, 2 MgSO47H20, 26 NaHCO3, and 10 Glucose) at a pH of 7.4. Borosilicate glass pipettes were pulled to resistances of ~7-12 MΩ and filled with internal solution (in mM: 135 K Gluconate, 7 NaCl, 10 HEPES, 2 MgCl2, 2 Na2ATP, and 0.3 Na2GTP). Cells were sealed to resistances of > 1GΩ. Following break in, cells were stimulated with step injections of 0.1nA from a holding potential of ~-60 - -100mV (as noted). Recordings from ~2-4 cells per condition per time point were analyzed.

Optical Induction

Blue light (470nm; ~2.4 mW/cm^2) was used to stimulate all cells. Commercially available LEDs were used to stimulate the first column of a 24-well plate and were on continuously for either 15 hours or 1 hour while a control group was kept in the dark. After testing gene induction with LEDs, micro-LEDs (Cree TR2227TM) were then used to create a defined spot of induction in HEK cells. LEDs were placed underneath each well, centered manually and turned on continuously for 8 hours. To optically induce Neurogenin and NeuroD, commercially available LEDs were used to expose NPCs that received the MMLV vector for 12 hrs. Reporter gene expression (YFP or RFP) indicated successful optical induction. Imaging was performed after 48

hrs for YFP expression or 72 hrs for RFP expression. Images were obtained using a Nikon Eclipse TE2000-U inverted microscope or a Nikon A1 Turf microscope.

Results

Our results indicate successful reprogramming of glia into functional neurons (Figure 1.1-1.2), light-induced gene expression (Figure 1.3), and optically-induced expression of proneural genes (Figure 1.4). Combined with recent efforts to deliver viral vectors surrounding implanted electrode arrays (not shown), we have developed strategies to reprogram the identity of cells surrounding electrode arrays and pattern their fate in response to light.

Glial reprogramming

We have successfully converted astrocytes to functional neurons using viral factor delivery. For our initial approach, we cultured primary rat cortical astrocytes and tested the delivery of a variety of proneural factors to the cells. Astrocytes are the most abundant cell type in the brain, and recent reports validate successful reprogramming approaches for these cells both *in vitro* and *in vivo* (Heinrich et al. 2010; Guo et al. 2014). We viewed *Ascl1* as a promising candidate for a proneural reprogramming factor based on reports demonstrating success in converting both fibroblasts (Vierbuchen et al. 2010) and astrocytes (Heinrich et al. 2010) to neurons. Likewise, we were interested in the effects of *Neurogenin* and *NeuroD* based on previous experience using those factors to murine embryonic stem cells(Tong et al. 2010; Purcell et al. 2013). In addition to *Ascl1*, *NeuroD1*, and *Neurogenin2*, we also assayed the factors Pou3F2 and Dlx2 for their efficacy of neuronal conversion. Of these, *Ascl1* appeared especially promising based on its robust conversion of glia to cells bearing the morphology and marker expression consistent with a neuronal phenotype (synapsin(SYN) and βIII tubulin(TUJ1))(Figure 1.1). Furthermore, these cells elicited spikes in response to injected current, which is a hallmark of neuronal function (Figure 1.2). Mature spike trains developed over a period of ~3 weeks in culture, with single spikes occurring ~1-2 weeks following factor delivery.

Combining Ascl1 with other factors did not yield a significant change in indicators of neural phenotype with the exception of Dlx2, that appeared to produce neurons with more mature characteristics (data not shown) combined with Ascl1 and cells that morphologically resembled neurons after prolonged (3-4 weeks) cultureWe are currently exploring the potential of this combination to accelerate maturation and control the functional phenotype of the cell (excitatory versus inhibitory fate (Heinrich et al. 2010)).

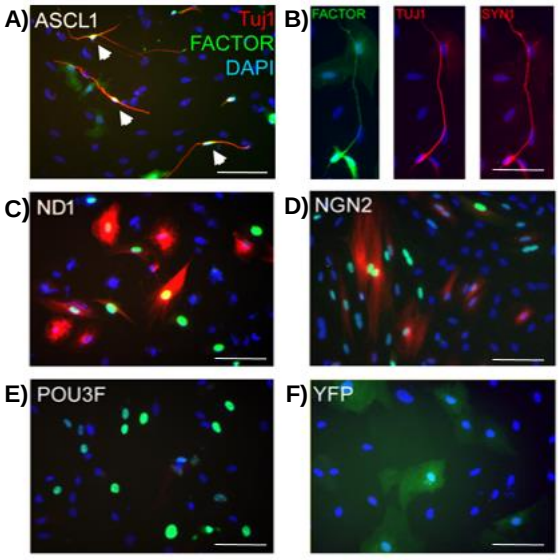

Figure 1.1. Reprogramming glia into neurons: histological evidence of neuronal conversion. Early observations indicate that the ASCL1 transgene is capable of producing cells with neuronal morphology and marker expression (TUJ1, SYN) from astrocyte cultures (a-b). Delivery of NeuroD1 (ND1) or Neurogenin-2 (NGN2) produced TUJ1 positivity (red) without accompanying morphological changes. POU3F and control YFP-infected cultures exhibited no observable conversion to neuronal fate. Scale = 5 um

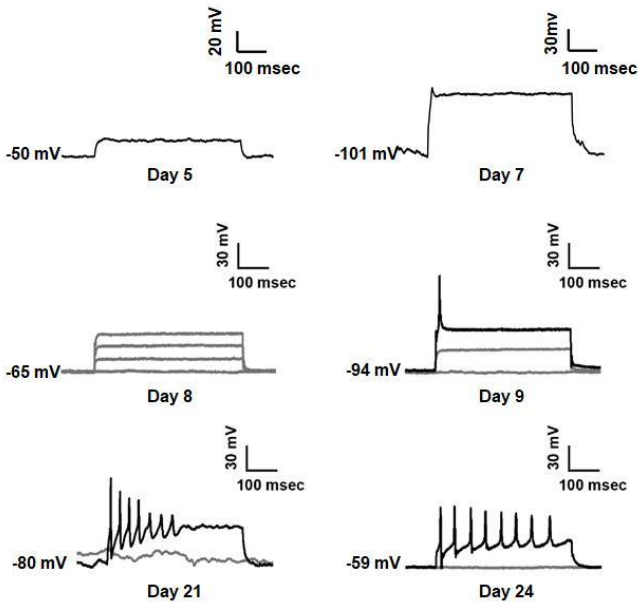

Figure 1.2. Reprogramming glia into neurons: electrophysiological evidence of neuronal conversion. Reprogrammed astrocytes were capable of eliciting a single spike in response to injected current by Day 9 post-infection, repetitive spiking by Day 21, and mature spike trains by Day 24 (representative traces). Earlier time points were consistently devoid of spiking activity. Control cultures displayed typical glial morphology and were likewise non-responsive to stimulation (not shown).

Optical Induction of Proneural Genes

Validation of the E222-based system. Experiments confirmed that the EL222 system was stably expressed in HEK cells transduced with a 4:1 ratio of reporter to activator plasmids produced robust expression of fluorescent reporter genes in response to light exposure (Figure 1.3). Notably, cells with increased proximity to the light source, or those exposed for longer periods of time, displayed an increase in reporter expression (Figure 1.3a). Spatial patterning of gene expression could be achieved either by the use of microscale LEDs (Figure 1.3b) or a photomask (Figure 1.3d). EL222 was successfully used to drive the expression of a variety of different reporter genes as described in Methods. In Figure 1.3b, YFP expression (green) identified cells which were successfully transfected with the EL222 system while RFP expression (red) indicated activation of the reporter by light. Alternatively, in Figure 1.3d, YFP was used as the reporter for light-driven gene expression.

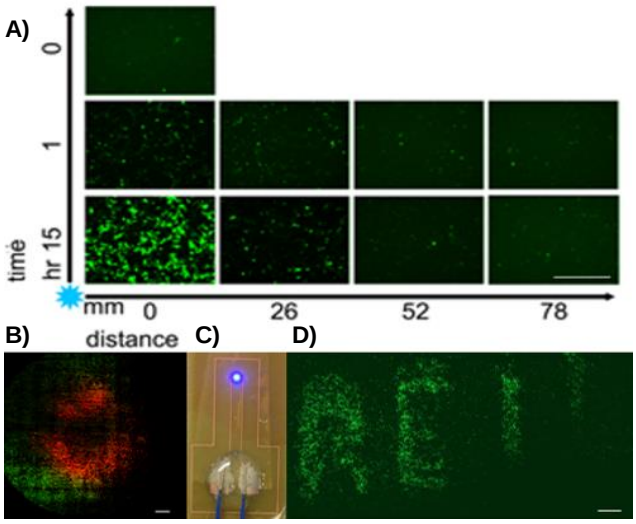

Figure 1.3. Successful light-induced gene expression with EL222 system. Increased light source proximity and longer exposure time led to a dose-dependent increase in reporter gene expression (YFP, green) (a). Two methods of spatial patterning of gene expression were achieved with the EL222 system: a spatially defined "spot" of RFP reporter induction (red, b) occurs in response to blue light delivered by a micro-LED (c), while a photomask "spells" the acronym for the lab (REIL) in YFP in response to blue light (d). Scales = 300 μm in (a), = 1mm in (b) and (d).

Light-Induced expression of proneural genes. Having validated the ability to drive reporter gene expression with EL222, we next coupled the system to the expression of fate-specifying genes. We tested the ability of our system to force expression of proneural genes in response to light in NPCs (Figure 1.4). NPCs have limited excitability despite morphological similarities with functional neurons and typically display immature spiking activity in response to injected current (Figure 1.4a). The EL222 system was tested to drive expression of NeuroD1 and Neurogenin2 in NPCs to produce neurons with enhanced morphologically maturity and electrically function. Our initial observations indicate that the EL222 system could drive detectable proneural gene expression after 12 hours of blue light exposure based on the observation of a the fused YFP tag (Figure 1.4b). No visible YFP expression was apparent in dark control cells, while those under light exposure show a significantly higher number of cells expressing the tagged fator. Future experiments will assess recording electrical activity at different time points from NPCs that have received NeuroD1 or Neurogenin2 and determine the effect of these proneural genes

on indicators of neural maturation. Combined with spatial patterning techniques (Figure 1.3), the data establish proof-of-principle for spatiotemporal control of neuronal fate-specifying genes in response to light.

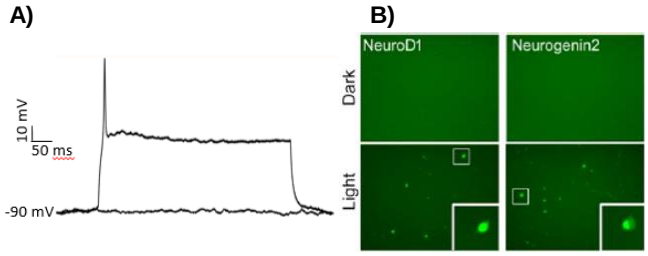

Figure 1.4. Optical control of proneural gene expression. Representative spike of a progenitor cell at day 9 of differentiation into neuron demonstrates limited excitability (a), which may be enhanced by proneural gene delivery. EL222 can drive proneural gene expression (YFP-tagged NeuroD1 or Neurogenin2 exposure, green) following 12 hrs of blue light exposure (b).

Discussion

MEAs implanted in the brain currently have substantial limitations related to suboptimal device-tissue integration. Our research group is developing novel techniques in cellular reprogramming and optogenetics to connect specific subpopulations of neurons with individual electrode sites: genetic engineering and light-driven stimuli will be used to dictate the connectivity between individual implanted electrode sites and specific subtypes of neurons. The end-goal is a fully-integrated abiotic-biotic interface capable of “tapping into” the electrical signals generated by specified brain circuitry. To meet this goal, we are pursuing two central strategies: (1) we are using replication-deficient viral vectors to reprogram identity of non-neuronal subtypes encapsulating the device toward neurons of specific identities, drawing from recent advances in cellular reprogramming and molecular biology(Heinrich et al. 2010; Vierbuchen et al. 2010; Guo et al. 2014), and (2) based on recent advances in optogenetics (Konermann et al. 2013; Motta-Mena et al. 2014), we are developing optical approaches to control neuronal identity via light-driven proneural gene expression. The goal is to regenerate and rewire the electrode interface, improving the stability and resolution of information transfer between neurons and electrodes.

Our data collected to-date provides proof-of-principle for producing functional neurons from non-neurons using our approaches (Figure 1.1-1.2), as well as achieving high spatiotemporal control over gene expression by coupling these strategies to light-activated transcription factors (Figure 1.3-1.4). Combined with confirmation that our gene expression system can be induced with light delivered by in-house assembled micro-LEDs (Figure 1.3c), we envision controlling the fate of cells at the interface of an integrated optoelectrode array (Khan and Li 2017) implanted in the brain in future work.

Acknowledgment

Melinda Frame from MSU's Center for Advanced Microscopy provided image acquisition training.

BIBLIOGRAPHY

BIBLIOGRAPHY

Adelman G, **Rane SG**, **Villa KF**. The cost burden of multiple sclerosis in the United States: a systematic review of the literature. *J Med Econ* 16: 639–647, 2013.

Anderson MA, **Ao Y**, **Sofroniew M V.** Heterogeneity of reactive astrocytes. *Neurosci Lett* 565: 23–29, 2014.

Anikeeva P, **Andalman AS**, **Witten I**, **Warden M**, **Goshen I**, **Grosenick L**, **Gunaydin LA**, **Frank LM**, **Deisseroth K**. Optetrode: a multichannel readout for optogenetic control in freely moving mice. *Nat Neurosci* 15: 163–70, 2011.

Arthur KC, **Calvo A**, **Price TR**, **Geiger JT**, **Chiò A**, **Traynor BJ**. Projected increase in amyotrophic lateral sclerosis from 2015 to 2040. *Nat Commun* 7: 12408, 2016.

Bedell HW, **Hermann JK**, **Ravikumar M**, **Lin S**, **Rein A**, **Li X**, **Molinich E**, **Smith PD**, **Selkirk SM**, **Miller RH**, **Sidik S**, **Taylor DM**, **Capadona JR**. Targeting CD14 on blood derived cells improves intracortical microelectrode performance. *Biomaterials* 163: 163–173, 2018.

Benabid AL, **Chabardes S**, **Torres N**, **Piallat B**, **Krack P**, **Fraix V**, **Pollak P**. Functional neurosurgery for movement disorders: a historical perspective. *Prog. Brain Res.* 175: 379–391, 2009.

Bennett C, **Samikkannu M**, **Mohammed F**, **Dietrich WD**, **Rajguru SM**, **Prasad A**. Blood brain barrier (BBB)-disruption in intracortical silicon microelectrode implants. *Biomaterials* 164: 1–10, 2018.

Biran R, **Martin DC**, **Tresco PA**. Neuronal cell loss accompanies the brain tissue response to chronically implanted silicon microelectrode arrays. *Exp Neurol* 195: 115–126, 2005.

Bouton CE, **Shaikhouni A**, **Annetta N V.**, **Bockbrader MA**, **Friedenberg DA**, **Nielson DM**, **Sharma G**, **Sederberg PB**, **Glenn BC**, **Mysiw WJ**, **Morgan AG**, **Deogaonkar M**, **Rezai AR**. Restoring cortical control of functional movement in a human with quadriplegia. *Nature* 533: 247–250, 2016.

Buffo A, **Rolando C**, **Ceruti S**. Astrocytes in the damaged brain: Molecular and cellular insights into their reactive response and healing potential. *Biochem Pharmacol* 79: 77–89, 2010.

Campbell A, **Wu C**, **Campbell A**, **Wu C**. Chronically Implanted Intracranial Electrodes: Tissue Reaction and Electrical Changes. *Micromachines* 9: 430, 2018.

Canales A, **Jia X**, **Froriep UP**, **Koppes RA**, **Tringides CM**, **Selvidge J**, **Lu C**, **Hou C**, **Wei L**, **Fink Y**, **Anikeeva P**. Multifunctional fibers for simultaneous optical, electrical and chemical interrogation of neural circuits in vivo. *Nat Biotechnol* 33: 277–284, 2015.

Cardin JA, **Carlén M**, **Meletis K**, **Knoblich U**, **Zhang F**, **Deisseroth K**, **Tsai L-H**, **Moore CI**. Targeted optogenetic stimulation and recording of neurons in vivo using cell-type-specific expression of Channelrhodopsin-2. *Nat Protoc* 5: 247–254, 2010.

Cavaglia M, **Dombrowski SM**, **Drazba J**, **Vasanji A**, **Bokesch PM**, **Janigro D**. Regional variation in brain capillary density and vascular response to ischemia. *Brain Res* 910: 81–93, 2001.

Chen R, **Canales A**, **Anikeeva P**. Neural recording and modulation technologies. *Nat Rev Mater* 2: 16093, 2017.

Chen Y, **Swanson RA**. Astrocytes and Brain Injury. *J Cereb Blood Flow Metab* 23: 137–149, 2003.

Chen Z-J, **Gillies GT**, **Broaddus WC**, **Prabhu SS**, **Fillmore H**, **Mitchell RM**, **Corwin FD**, **Fatouros PP**. A realistic brain tissue phantom for intraparenchymal infusion studies. *J Neurosurg* 101: 314–322, 2004.

Collinger JL, **Wodlinger B**, **Downey JE**, **Wang W**, **Tyler-Kabara EC**, **Weber DJ**, **McMorland AJ**, **Velliste M**, **Boninger ML**, **Schwartz AB**. High-performance neuroprosthetic control by an individual with tetraplegia. *Lancet* 381: 557–564, 2013.

Dorsey ER, **Constantinescu R**, **Thompson JP**, **Biglan KM**, **Holloway RG**, **Kieburtz K**, **Marshall FJ**, **Ravina BM**, **Schifitto G**, **Siderowf A**, **Tanner CM**. Projected number of people with Parkinson disease in the most populous nations, 2005 through 2030. *Neurology* 68: 384–386, 2007.

Downen M, **Amaral TD**, **Hua LL**, **Zhao M-L**, **Lee SC**. Neuronal death in cytokine-activated primary human brain cell culture: role of tumor necrosis factor-? *Glia* 28: 114–127, 1999.

Eles JR, **Vazquez AL**, **Kozai TDY**, **Cui XT**. In vivo imaging of neuronal calcium during electrode implantation: Spatial and temporal mapping of damage and recovery. *Biomaterials* 174: 79–94, 2018.

Ereifej ES, **Smith CS**, **Meade SM**, **Chen K**, **Feng H**, **Capadona JR**. The Neuroinflammatory Response to Nanopatterning Parallel Grooves into the Surface Structure of Intracortical Microelectrodes. *Adv Funct Mater* 28: 1704420, 2018.

Ezzyat Y, **Wanda PA**, **Levy DF**, **Kadel A**, **Aka A**, **Pedisich I**, **Sperling MR**, **Sharan AD**, **Lega BC**, **Burks A**, **Gross RE**, **Inman CS**, **Jobst BC**, **Gorenstein MA**, **Davis KA**, **Worrell GA**, **Kucewicz MT**, **Stein JM**, **Gorniak R**, **Das SR**, **Rizzuto DS**, **Kahana MJ**. Closed-loop stimulation of temporal cortex rescues functional networks and improves memory. *Nat Commun* 9: 365, 2018.

Golabchi A, **Wu B**, **Li X**, **Carlisle DL**, **Kozai TDY**, **Friedlander RM**, **Cui XT**. Melatonin improves quality and longevity of chronic neural recording. *Biomaterials* 180: 225–239, 2018.

Greenberg PE, **Kessler RC**, **Birnbaum HG**, **Leong SA**, **Lowe SW**, **Berglund PAA**, **Corey-Lisle PK**. The Economic Burden of Depression in the United States: How Did It Change Between 1990 and 2000? *J Clin Psychiatry* 64: 1465–1475, 2003.

Guo Z, **Zhang L**, **Wu Z**, **Chen Y**, **Wang F**, **Chen G**. In Vivo Direct Reprogramming of Reactive Glial Cells into Functional Neurons after Brain Injury and in an Alzheimer's Disease Model. *Cell Stem Cell* 14: 188–202, 2014.

Halpern CH, **Samadani U**, **Litt B**, **Jaggi JL**, **Baltuch GH**. Deep Brain Stimulation for Epilepsy. In: *Neuromodulation*. Elsevier, p. 639–649.

Hascup KN, **Hascup ER**, **Stephens ML**, **Glaser PEA**, **Yoshitake T**, **Mathé AA**, **Gerhardt GA**, **Kehr J**. Resting glutamate levels and rapid glutamate transients in the prefrontal cortex of the Flinders Sensitive Line rat: a genetic rodent model of depression. *Neuropsychopharmacology* 36: 1769–77, 2011.

He W, **Bellamkonda R V.** A Molecular Perspective on Understanding and Modulating the Performance of Chronic Central Nervous System (CNS) Recording Electrodes [Online]. CRC Press/Taylor & Francis. http://www.ncbi.nlm.nih.gov/pubmed/21204400 [31 Oct. 2018].

Heinrich C, **Blum R**, **Gascón S**, **Masserdotti G**, **Tripathi P**, **Sánchez R**, **Tiedt S**, **Schroeder T**, **Götz M**, **Berninger B**. Directing Astroglia from the Cerebral Cortex into Subtype Specific Functional Neurons. *PLoS Biol* 8: e1000373, 2010.

Igarashi H, **Koizumi K**, **Kaneko R**, **Ikeda K**, **Egawa R**, **Yanagawa Y**, **Muramatsu S**, **Onimaru H**, **Ishizuka T**, **Yawo H**. A Novel Reporter Rat Strain That Conditionally Expresses the Bright Red Fluorescent Protein tdTomato. *PLoS One* 11: e0155687, 2016.

Jennings JH, **Stuber GD**. Tools for Resolving Functional Activity and Connectivity within Intact Neural Circuits. *Curr Biol* 24: R41–R50, 2014.

Jeong J-W, **McCall JG**, **Shin G**, **Zhang Y**, **Al-Hasani R**, **Kim M**, **Li S**, **Sim JY**, **Jang K-I**, **Shi Y**, **Hong DY**, **Liu Y**, **Schmitz GP**, **Xia L**, **He Z**, **Gamble P**, **Ray WZ**, **Huang Y**, **Bruchas MR**, **Rogers JA**. Wireless Optofluidic Systems for Programmable In Vivo Pharmacology and Optogenetics. *Cell* 162: 662–674, 2015.

Jorfi M, **Skousen JL**, **Weder C**, **Capadona JR**. Progress towards biocompatible intracortical microelectrodes for neural interfacing applications. *J Neural Eng* 12: 011001, 2015.

Karumbaiah L, **Saxena T**, **Carlson D**, **Patil K**, **Patkar R**, **Gaupp EA**, **Betancur M**, **Stanley GB**, **Carin L**, **Bellamkonda R V.** Relationship between intracortical electrode design and chronic recording function. *Biomaterials* 34: 8061–8074, 2013.

Khan W, **Li W**. Wafer level fabrication method of hemispherical reflector coupled micro-led array stimulator for optogenetics. In: *2017 19th International Conference on Solid-State Sensors, Actuators and Microsystems (TRANSDUCERS)*. IEEE, p. 2231–2234.

Konermann S, **Brigham MD**, **Trevino A**, **Hsu PD**, **Heidenreich M**, **Cong L**, **Platt RJ**, **Scott DA**, **Church GM**, **Zhang F**. Optical control of mammalian endogenous transcription and epigenetic states. *Nature* 500: 472–476, 2013.

Kowal SL, **Dall TM**, **Chakrabarti R**, **Storm M V.**, **Jain A**. The current and projected economic burden of Parkinson's disease in the United States. *Mov Disord* 28: 311–318, 2013.

Kozai TDY, **Catt K**, **Li X**, **Gugel Z V.**, **Olafsson VT**, **Vazquez AL**, **Cui XT**. Mechanical failure modes of chronically implanted planar silicon-based neural probes for laminar recording. *Biomaterials* 37: 25–39, 2015a.

Kozai TDY, **Gugel Z**, **Li X**, **Gilgunn PJ**, **Khilwani R**, **Ozdoganlar OB**, **Fedder GK**, **Weber DJ**,

Cui XT. Chronic tissue response to carboxymethyl cellulose based dissolvable insertion needle for ultra-small neural probes. *Biomaterials* 35: 9255–9268, 2014.

Kozai TDY, **Jaquins-Gerstl AS**, **Vazquez AL**, **Michael AC**, **Cui XT**. Brain tissue responses to neural implants impact signal sensitivity and intervention strategies. *ACS Chem Neurosci* 6: 48–67, 2015b.

Kozai TDY, **Jaquins-Gerstl AS**, **Vazquez AL**, **Michael AC**, **Cui XT**. Dexamethasone retrodialysis attenuates microglial response to implanted probes in vivo. *Biomaterials* 87: 157–169, 2016.

Kozai TDY, **Langhals NB**, **Patel PR**, **Deng X**, **Zhang H**, **Smith KL**, **Lahann J**, **Kotov NA**, **Kipke DR**. Ultrasmall implantable composite microelectrodes with bioactive surfaces for chronic neural interfaces. *Nat Mater* 11: 1065–1073, 2012.

Lebedev MA, **Nicolelis MAL**. Brain–machine interfaces: past, present and future. *Trends Neurosci* 29: 536–546, 2006.

Lee M, **Schwab C**, **Mcgeer PL**. Astrocytes are GABAergic cells that modulate microglial activity. *Glia* 59: 152–165, 2011.

Liddelow SA, **Guttenplan KA**, **Clarke LE**, **Bennett FC**, **Bohlen CJ**, **Schirmer L**, **Bennett ML**, **Münch AE**, **Chung W-S**, **Peterson TC**, **Wilton DK**, **Frouin A**, **Napier BA**, **Panicker N**, **Kumar M**, **Buckwalter MS**, **Rowitch DH**, **Dawson VL**, **Dawson TM**, **Stevens B**, **Barres BA**. Neurotoxic reactive astrocytes are induced by activated microglia. *Nature* 541: 481–487, 2017.

Ludwig K a, **Uram JD**, **Yang J**, **Martin DC**, **Kipke DR**. Chronic neural recordings using silicon microelectrode arrays electrochemically deposited with a poly(3,4-ethylenedioxythiophene) (PEDOT) film. *J Neural Eng* 3: 59–70, 2006.

Ludwig KA, **Miriani RM**, **Langhals NB**, **Joseph MD**, **Anderson DJ**, **Kipke DR**. Using a Common Average Reference to Improve Cortical Neuron Recordings From Microelectrode Arrays. *J Neurophysiol* 101: 1679–1689, 2009.

Malaga KA, **Schroeder KE**, **Patel PR**, **Irwin ZT**, **Thompson DE**, **Bentley JN**, **Lempka SF**, **Chestek CA**, **Patil PG**. Data-driven model comparing the effects of glial scarring and interface interactions on chronic neural recordings in non-human primates. *J Neural Eng J Neural Eng* 13: 16010–16024, 2016.

Malone DA, **Dougherty DD**, **Rezai AR**, **Carpenter LL**, **Friehs GM**, **Eskandar EN**, **Rauch SL**, **Rasmussen SA**, **Machado AG**, **Kubu CS**, **Tyrka AR**, **Price LH**, **Stypulkowski PH**, **Giftakis JE**, **Rise MT**, **Malloy PF**, **Salloway SP**, **Greenberg BD**. Deep Brain Stimulation of the Ventral Capsule/Ventral Striatum for Treatment-Resistant Depression. *Biol Psychiatry* 65: 267–275, 2009.

Mayberg HS, **Lozano AM**, **Voon V**, **McNeely HE**, **Seminowicz D**, **Hamani C**, **Schwalb JM**, **Kennedy SH**. Deep Brain Stimulation for Treatment-Resistant Depression. *Neuron* 45: 651–660, 2005.

McCreery D, **Cogan S**, **Kane S**, **Pikov V**. Correlations between histology and neuronal activity recorded by microelectrodes implanted chronically in the cerebral cortex. *J Neural Eng* 13:

036012, 2016.

Michelson NJ, **Vazquez AL**, **Eles JR**, **Salatino JW**, **Purcell EK**, **Williams JJ**, **Cui XT**, **Kozai TDY**. Multi-scale, multi-modal analysis uncovers complex relationship at the brain tissue-implant neural interface: new emphasis on the biological interface. *J Neural Eng* 15: 033001, 2018.
Motta-Mena LB, **Reade A**, **Mallory MJ**, **Glantz S**, **Weiner OD**, **Lynch KW**, **Gardner KH**. An optogenetic gene expression system with rapid activation and deactivation kinetics. *Nat Chem Biol* 10: 196–202, 2014.

Nagy A. Cre recombinase: The universal reagent for genome tailoring. *genesis* 26: 99–109, 2000.

Nolta NF, **Christensen MB**, **Crane PD**, **Skousen JL**, **Tresco PA**. BBB leakage, astrogliosis, and tissue loss correlate with silicon microelectrode array recording performance. *Biomaterials* 53: 753–762, 2015.

O'Doherty JE, **Lebedev MA**, **Ifft PJ**, **Zhuang KZ**, **Shokur S**, **Bleuler H**, **Nicolelis MAL**. Active tactile exploration using a brain-machine-brain interface. *Nature* 479: 228–31, 2011.

Oakes RS, **Polei MD**, **Skousen JL**, **Tresco PA**. An astrocyte derived extracellular matrix coating reduces astrogliosis surrounding chronically implanted microelectrode arrays in rat cortex. *Biomaterials* 154: 1–11, 2018.

Perry VH, **Teeling J**. Microglia and macrophages of the central nervous system: the contribution of microglia priming and systemic inflammation to chronic neurodegeneration. *Semin Immunopathol* 35: 601–12, 2013.

Polikov VS, **Tresco PA**, **Reichert WM**. Response of brain tissue to chronically implanted neural electrodes. *J Neurosci Methods* 148: 1–18, 2005.

Potter KA, **Buck AC**, **Self WK**, **Callanan ME**, **Sunil S**, **Capadona JR**. The effect of resveratrol on neurodegeneration and blood brain barrier stability surrounding intracortical microelectrodes. *Biomaterials* 34: 7001–7015, 2013.

Purcell EK, **Thompson DE**, **Ludwig KA**, **Kipke DR**. Flavopiridol reduces the impedance of neural prostheses in vivo without affecting recording quality. *J Neurosci Methods* 183: 149–157, 2009.

Purcell EK, **Yang A**, **Liu L**, **Velkey JM**, **Morales MM**, **Duncan RK**. BDNF profoundly and specifically increases KCNQ4 expression in neurons derived from embryonic stem cells. *Stem Cell Res* 10: 29–35, 2013.

Ralay Ranaivo H, **Wainwright MS**. Albumin activates astrocytes and microglia through mitogen-activated protein kinase pathways. *Brain Res* 1313: 222–31, 2010.

Rennaker RL, **Miller J**, **Tang H**, **Wilson DA**. Minocycline increases quality and longevity of chronic neural recordings. *J Neural Eng* 4: L1-5, 2007.

Rosin B, **Slovik M**, **Mitelman R**, **Rivlin-Etzion M**, **Haber SN**, **Israel Z**, **Vaadia E**, **Bergman H**. Closed-Loop Deep Brain Stimulation Is Superior in Ameliorating Parkinsonism. *Neuron* 72: 370–384, 2011.

Rossi JL, **Ralay Ranaivo H**, **Patel F**, **Chrzaszcz M**, **Venkatesan C**, **Wainwright MS**. Albumin causes increased myosin light chain kinase expression in astrocytes via p38 mitogen-activated protein kinase. *J Neurosci Res* 89: 852–61, 2011.

Salatino JW, **Ludwig KA**, **Kozai TDY**, **Purcell EK**. Glial responses to implanted electrodes in the brain. *Nat Biomed Eng* 1: 862–877, 2017a.

Salatino JW, **Winter BM**, **Drazin MH**, **Purcell EK**. Functional remodeling of subtype-specific markers surrounding implanted neuroprostheses. *J Neurophysiol* 118: 194–202, 2017b.

Seidl K, **Spieth S**, **Herwik S**, **Steigert J**, **Zengerle R**, **Paul O**, **Ruther P**. In-plane silicon probes for simultaneous neural recording and drug delivery. *J Micromechanics Microengineering* 20: 105006, 2010.

Seymour JP, **Kipke DR**. Neural probe design for reduced tissue encapsulation in CNS. *Biomaterials* 28: 3594–3607, 2007.

Shen Q, **Rigor RR**, **Pivetti CD**, **Wu MH**, **Yuan SY**. Myosin light chain kinase in microvascular endothelial barrier function. *Cardiovasc Res* 87: 272–80, 2010.

Shen W, **Karumbaiah L**, **Liu X**, **Saxena T**, **Chen S**, **Patkar R**, **Bellamkonda R V.**, **Allen MG**. Extracellular matrix-based intracortical microelectrodes: Toward a microfabricated neural interface based on natural materials. *Microsystems Nanoeng* 1: 15010, 2015.

Sofroniew M V. Molecular dissection of reactive astrogliosis and glial scar formation. *Trends Neurosci* 32: 638–47, 2009.

Sofroniew M V. Astrogliosis. *Cold Spring Harb Perspect Biol* 7: a020420, 2014.

Sofroniew M V, **Vinters H V**. Astrocytes: biology and pathology. *Acta Neuropathol* 119: 7–35, 2010.

Sommakia S, **Lee HC**, **Gaire J**, **Otto KJ**. Materials approaches for modulating neural tissue responses to implanted microelectrodes through mechanical and biochemical means. *Curr Opin Solid State Mater Sci* 18: 319–328, 2014.

Suo Z, **Wu M**, **Citron BA**, **Gao C**, **Festoff BW**. Persistent protease-activated receptor 4 signaling mediates thrombin-induced microglial activation. *J Biol Chem* 278: 31177–83, 2003.

Tong M, **Hernandez JL**, **Purcell EK**, **Altschuler RA**, **Duncan RK**. The intrinsic electrophysiological properties of neurons derived from mouse embryonic stem cells overexpressing neurogenin-1. *Am J Physiol Physiol* 299: C1335–C1344, 2010.

Vierbuchen T, **Ostermeier A**, **Pang ZP**, **Kokubu Y**, **Südhof TC**, **Wernig M**. Direct conversion of fibroblasts to functional neurons by defined factors. *Nature* 463: 1035–1041, 2010.

Volterra A, **Meldolesi J**. Astrocytes, from brain glue to communication elements: the revolution continues. *Nat Rev Neurosci* 6: 626–640, 2005.

Weaver FM, **Follett K**, **Stern M**, **Hur K**, **Harris C**, **Marks WJ**, **Rothlind J**, **Sagher O**, **Reda D**,

Moy CS, **Pahwa R**, **Burchiel K**, **Hogarth P**, **Lai EC**, **Duda JE**, **Holloway K**, **Samii A**, **Horn S**, **Bronstein J**, **Stoner G**, **Heemskerk J**, **Huang GD**, **Group for the C 468 S**, **KA F**, **S M**, **J C**, **RL R**, **F W**, **AE L**, **Y T**, **P K**, **G D**, **MM H**, **JW L**, **MF F**, **S F**, **RS S**, **V P**, **RA H**, **CG G**, **R P**, **A S**, **K S-T**, **H J**, **P L**, **K W**, **M A**, **BS A**, **Y T**, **KJ B**, **MI H**. Bilateral Deep Brain Stimulation vs Best Medical Therapy for Patients With Advanced Parkinson Disease<subtitle>A Randomized Controlled Trial</subtitle> *JAMA* 301: 63, 2009.

Weinstein JR, **Gold SJ**, **Cunningham DD**, **Gall CM**, **Sastre A**, **Lyuboslavsky P**, **Hepler JR**, **McKeon RJ**, **Traynelis SF**. Cellular localization of thrombin receptor mRNA in rat brain: expression by mesencephalic dopaminergic neurons and codistribution with prothrombin mRNA. *J Neurosci* 15: 2906–19, 1995.

Wellman SM, **Eles JR**, **Ludwig KA**, **Seymour JP**, **Michelson NJ**, **McFadden WE**, **Vazquez AL**, **Kozai TDY**. A Materials Roadmap to Functional Neural Interface Design. *Adv Funct Mater* 28: 1701269, 2018.

Wimo A, **Jönsson L**, **Bond J**, **Prince M**, **Winblad B**, **Alzheimer Disease International**. The worldwide economic impact of dementia 2010. *Alzheimers Dement* 9: 1–11.e3, 2013.

Winter B, **Daniels S**, **Salatino J**, **Purcell E**. Genetic Modulation at the Neural Microelectrode Interface: Methods and Applications. *Micromachines 2018, Vol 9, Page 476* 9: 476, 2018.

Winter BM, **Setien MB**, **Salatino JW**, **Blanke N**, **Thompson CH**, **Smith KR**, **Khan WA**, **Li W**, **Suhr ST**, **Purcell EK**. Control of cell fate and excitability at the neural electrode interface: Genetic reprogramming and optical induction. In: *2017 IEEE Life Sciences Conference (LSC)*. IEEE, p. 157–161.

Zamanian JL, **Xu L**, **Foo LC**, **Nouri N**, **Zhou L**, **Giffard RG**, **Barres BA**. Genomic analysis of reactive astrogliosis. *J Neurosci* 32: 6391–410, 2012.

CHAPTER 2 Genetic modulation at the neural microelectrode interface: methods and applications

Introduction

Increasing prevalence of patients affected by neurodegenerative diseases and psychiatric disorders places an economic, social, and psychological burden on society(Greenberg et al. 2003; Dorsey et al. 2007; Adelman et al. 2013; Kowal et al. 2013; Wimo et al. 2013; Arthur et al. 2016). In research settings, there has been a significant rise in the use of microelectrodes implanted in the brain to record neural activity and reveal the underlying mechanisms of these diseases. Moreover, brain machine interfaces (BMIs) and closed-loop deep brain stimulation (DBS) are emerging applications of recording arrays in preclinical and clinical trials(Lebedev and Nicolelis 2006; Hascup et al. 2011; O'Doherty et al. 2011; Rosin et al. 2011; Ezzyat et al. 2018). However, signal quality is notoriously unstable and prone to loss over time, undermining the efficacy of decoding algorithms, the accuracy of data collection in basic science studies, and the detection of conditioning signals necessary to drive closed-loop strategies(Kozai et al. 2014; Nolta et al. 2015; McCreery et al. 2016; Salatino et al. 2017a). The brain initiates a tissue response following implantation that is characterized by progressive glial encapsulation and neuronal loss, which is widely believed to contribute to diminished recording quality and signal loss(Jorfi et al. 2015; Kozai et al. 2015b; Salatino et al. 2017a). Still, despite recent findings, both the nature of the relationship between the tissue response and recording quality, as well as the underlying mechanisms responsible, remain unclear(Michelson et al. 2018).

In recent years, an increasingly complex view of the tissue response to neural implants has emerged, where changes in the structure and function of responding cell types accompanies well-known effects on cellular density (glial encapsulation and local loss of neurons). Recent evidence suggests that local shifts in ion channel expression, synaptic transporter expression, and astrocyte subtype follow device implantation(Salatino et al. 2017a, 2017b). Additionally, Eles *et al*. noted new evidence that mechanical trauma accompanies prolonged, localized

calcium influx post-implantation(Eles et al. 2018). For non-neuronal responses, a recent study employed a mouse bone marrow chimera model as an innovative approach to delineate the roles of resident microglia versus blood-derived macrophages in determining microelectrode performance. The study revealed that knockout of CD14 from blood-derived macrophages improved recording quality over 16 weeks(Bedell et al. 2018). Further, new approaches using extracellular matrix-based intracortical arrays have reduced inflammatory responses, demonstrating the important role of acellular elements in modulating the tissue response(Shen et al. 2015; Oakes et al. 2018). While these findings provide insight on the fundamental mechanisms of the tissue response, they also illustrate the complexity of device-tissue interactions and the significant unknowns that remain with respect to the signaling pathways responsible.

Advances in the development of new genetic tools provide opportunities to identify the precise pathways of cellular responses, where devices are being designed and fabricated with increasingly sophisticated means of delivering the necessary reagents to surrounding tissue. Multifunctional microelectrode arrays offer the ability to interrogate cellular events surrounding the device via electrical, chemical, and optical modes of stimulation(Seidl et al. 2010; Anikeeva et al. 2011; Canales et al. 2015; Jeong et al. 2015), and integrated microfluidic channels permit vector delivery for genetic modification of the local neural network(Jennings and Stuber 2014; Jeong et al. 2015). The resulting upregulation or downregulation of specific signaling pathways is a potentially powerful means of investigating the mechanisms of the tissue response. However, difficulties can arise in chronic settings, since biofouling and tissue ingrowth can compromise the patency of the infusion channel, making repeated dosing and/or vector delivery at long-term time points challenging(Sommakia et al. 2014; Jeong et al. 2015; Chen et al. 2017). Here, we present data illustrating proof-of-principle for delivering vectors capable of modifying gene expression (siRNA and viral vectors) via a functional microfluidic device capable of recording neural activity in the primary motor cortex of adult rats. By delivering DNA or RNA

constructs designed for gene knockdown (BLOCK-iT™ siRNA, Thermo Fischer), overexpression (AAV8-GFAP-mCherry, UNC Vector Core), and conditional expression (AAV2-Cre-GFP, Vector Biolabs), our results provide methodology for genetic modification of the tissue response at the neural-electrode interface.

Materials and Methods

Injection Protocol (in vitro)

The workflow of the injection protocol developed is illustrated in Figure 2.1A. A custom 16-channel single shank microfluidic microelectrode array (Neuronexus) was pre-threaded with a 40 gauge SS316L wire (KidneyPuncher). Due to the slight bend in the microfluidic channel near the electrical connector (Figure 2.1F), an infusion cannula (33 gauge internal cannula, C315LI/SPC PlasticsOne) was used as a guide for the wire insert. For initial *in vitro* testing and methods development, the MEA was inserted into a brain tissue phantom consisting of a 0.6% agarose hydrogel cast into a 10cm cell culture petri dish and held in place using a hemostat and C-clamps (Figure 2.1B-C)(Chen et al. 2004). Subsequently, the wire was inserted 1mm past the tip of the MEA into the agarose medium to clear the microfluidic channel and reduce back pressure. To infuse, the infusion cannula was first attached to a 10uL Hamilton syringe with 7cm of silicon tubing (C313CT, PlasticsOne). Using a Quintessential Stereotaxic Injector (Stoelting), 4µL of mineral oil was withdrawn at 0.1µL/min, followed by 2µL of air, and finally 2µL of saline tinted with fast green (Electron Microscopy Sciences) at the same rate. Using hemostats, the cannula was carefully inserted into the microfluidic channel and glued in place. The saline was then infused into the agarose medium at a rate of 0.1µL/min (a standard infusion rate for vector injection into brain tissue)(Cardin et al. 2010).

Adapter Circuit

Due to the close proximity of the microfluidic channel, an adapter circuit was designed and fabricated to allow added clearance between the connector and infusion channel and facilitate the collection of neural recording data. Using EAGLE schematic software (Autodesk), the circuit board was designed to extend the connection site 1 inch away from the device (fabricated by

Gold Phoenix PCB) (Figure 2.1D-E). Electrical connectors (Omnetics) with through-hole style leads were chosen for ease of assembly, and connection pads were determined based on manufacturer specifications.

Surgical Procedure

For conditional expression, we purchased a reporter rat strain from the National BioResource Project (Kyoto University) which enables high-resolution imaging of dendritic spines in *ex vivo* brain slices(Igarashi et al. 2016). For the reporter strain, female Long Evans rats were generated with a floxed STOP tdTomato to allow conditional expression of the red fluorescent reporter via viral delivery of Cre recombinase (4.0E12 GC/mL AAV2-Cre-GFP in 5% Glycerol in PBS, Vector Biolabs). For overexpression and knockdown studies, adult male Sprague-Dawley rats (Charles River) were delivered an AAV vector with a GFAP promoter and mCherry reporter (AAV8-GFAP-mCherry 2.7E12 virus molecules/ mL in 350nM NaCl and 5% D-Sorbitol in PBS, UNC Vector Core) and BLOCK-iT^{TM} siRNA (200nM Invivofectamine-BLOCK-iT^{TM}-Complexation solution, Thermo Fisher) respectively. Animals were unilaterally implanted in the motor cortex with a commercially manufactured 16-channel single shank MEA with a microfluidic channel (NeuroNexus) that was pre-threaded with a 40 gauge SS316L wire (KidneyPuncher) based on previously published methods using single shank standard (non-microfluidic) Michigan arrays(Salatino et al. 2017b). The majority of the implanted microfluidic devices were nonfunctional. All devices were modified so that the plastic tubing was ~2cm long. Animals were anesthetized with ~2% isoflurane throughout the surgery. Using a motorized drill, a 2x2mm craniotomy was performed to expose the cortex (3mm anterior, 2.5mm lateral to bregma). The dura was resected and the MEA was implanted at a 2mm depth in the cortex. Subsequently, the wire was manually threaded and inserted ~1mm past the tip of the MEA. A dental acrylic headcap anchored by three bones screws was used to support the MEA. Excess dental acrylic was used to attach the wire to the plastic tubing of the microfluidic channel. Bupivacaine was administered for topical analgesia at the wound site, and meloxicam was administered for systemic analgesia via intraperitoneal injection during

recovery. All surgical procedures were approved by the Michigan State University Animal Care and Use Committee.

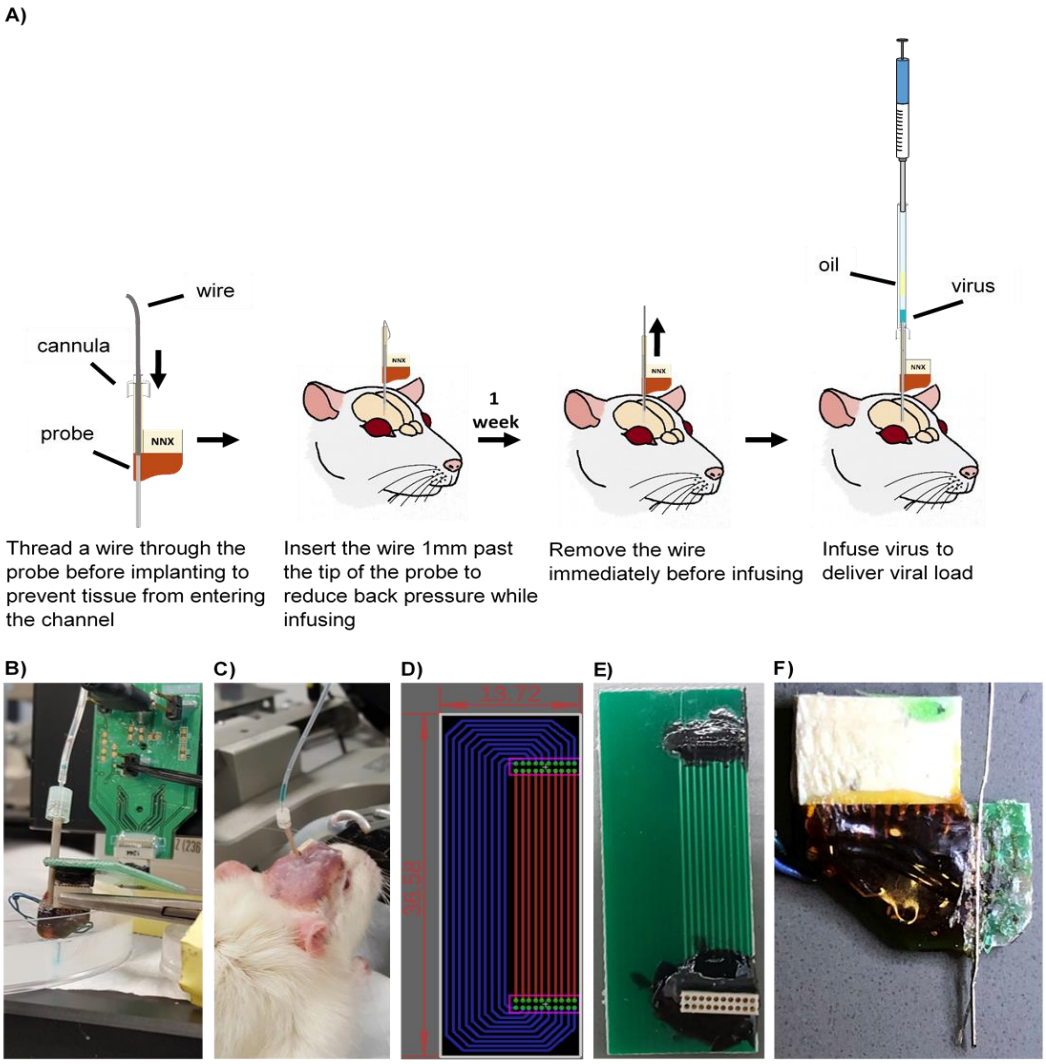

Figure 2.1. Implanting and infusing through the microfluidic device. A) Microfluidic device implantation and infusion protocol **B)** *In vitro* saline infusion into 0.6% agarose. Saline was tinted with fast green to confirm delivery. Inset displays the microfluidic device **C)** *In vivo* infusion of AAV8 viral load **D)** Top view of the adapter board layout. Green circles indicate the plated through-holes through which the electrical connector (Omnetics) leads are inserted. Electrical traces were placed on the top (red) and bottom (blue) to prevent traces from overlapping. Dimensions indicated in the figure are in millimeters. **E)** Fabricated adapter board **F)** Cross section of a microfluidic probe. Red arrow indicates a slight bend in the microfluidic channel.

Injection Protocol (in vivo)

Animals were infused 1-3 weeks post-implantation. Animals were anesthetized with ~2% isoflurane for the duration of the procedure. Oil, air and 2 µL of viral load were withdrawn as described in the Injection Protocol section. The wire was removed from the microfluidic channel and the cannula was inserted using hemostats and glued in place. The viral load was infused at 0.2-0.4 µL/min. For troubleshooting techniques, see Box 1.

Box 1
Troubleshooting Techniques

The channel becomes clogged

If the wire insert is pulled out, tissue can infiltrate and clog the microfluidic channel, preventing successful infusion. In order to clear the channel, a new wire must be inserted; however, a blunt wire may not be able to pierce through the debris. Filing the tip of the wire to a point can help clear the debris from the channel and may require multiple attempts.

The plastic tubing breaks off

The plastic tubing can be damaged or completely broken through contact with the environment as the animal explores its cage. If the plastic tubing can be recovered from the enclosure, it can be reattached with super glue immediately before infusing. If the tubing cannot be recovered, a guide cannula (PlasticsOne) can be used as a substitute.

The microfluidic channel becomes damaged

If the plastic tubing is broken, the microfluidic channel can become damaged or removed as well. If a portion of the microfluidic channel is still attached, straighten the channel out and reattach or replace the plastic tubing. If the microfluidic channel has broken off completely, the channel has to be reconstructed. First, ensure the microfluidic channel is clear of debris. Thread a cannula with a wire insert and insert the cannula into the plastic tubing/guide cannula until the ends are aligned. Extend the wire far enough past the opening that it can be easily manipulated. Using forceps, guide the wire into the microfluidic channel to align the cannula and plastic tubing/guide cannula. Apply super glue to the bottom of the plastic tubing/guide cannula and allow it to set. Finally, remove the cannula and wire insert.

The virus will not infuse

If the virus will not infuse, it is possible that the wire was not inserted far enough and the channel is blocked with tissue. Re-insert a wire through the channel until it extends approximately one millimeter past the end of the microfluidic channel. If the virus still will not infuse, increase the infusion rate slightly until successful.

Immunohistochemistry

Two to three weeks post-injection, animals were deeply anesthetized with an overdose of sodium pentobarbital and transcardially perfused with 4% paraformaldehyde (PFA). Brains were extracted, stored in 4% PFA overnight and cryoembedded following sucrose protection. Cryosections were collected at a 20µm thickness and hydrated with PBS prior to blocking in 10% normal goat serum in PBS for 1 hour. Tissue subsequently was incubated at 4°C with

mouse anti-glial fibrillary acidic protein (GFAP) (Cell Signaling Technology) overnight. The following day, cryosections were rinsed with PBS and incubated with goat anti-mouse IgG (H+L) Alexa Fluor 488 conjugate (1:200, Thermo Fisher Scientific, Waltham, MA) for two hours at room temperature. Finally, nuclei were counterstained with Hoechst and coverslipped with ProLong Gold antifade reagent (Fisher Scientific Company). An Olympus Fluoview 1000 inverted confocal microscope was used to image samples with a 20x PlanFluor dry objective (0.5NA). For comparison, GFAP-stained tissue from “traditional” (non-microfluidic) single shank Michigan-style arrays implanted in motor cortex was assessed using images collected during a previous study (Purcell et al. 2009).

Image Analysis

All images were analyzed using a MATLAB script adapted from Kozai et al. (Kozai et al. 2014) with modifications previously reported (Salatino et al. 2017b). A hand-traced outline of the injury was used to define concentric 10μm-thick bins. The average intensity of the fluorescent markers within each bin was calculated using the corners of the image as a reference. Bin intensity was normalized to the most distal bin. Results were assessed using a mixed model ANOVA and SPSS software (IBM, Chicago, IL) as previously described(Salatino et al. 2017b).

Signal Processing

Neural recording data were acquired with a Tucker-Davis Technologies RZ2 system (Alchua, FL) and processed using a MATLAB script. Wideband data was sampled at ~48 kHz in isoflurane-anesthetized rats placed in a Faraday cage and analyzed offline as described(Ludwig et al. 2006; Purcell et al. 2009), where a combination of bandpass filtering and identification of threshold crossings (at 3.5 standard deviations from the mean of the sampling distribution) were used to collect and store 3 msec snippets centered at the minimum of the recorded segment. Local field potentials (LFPs) were filtered between 1-100 Hz. LFP amplitude was calculated by multiplying the standard deviation of the signal by six, yielding 99.7% of the signal amplitude. Principal component analysis and fuzzy C-means clustering (membership index>0.8) were performed to identify putative units in combination with visual inspection of mean waveforms.

Common average referencing(Ludwig et al. 2009) was used to mitigate noise sources common to every electrode site (such as line noise and movement artifacts).

Results

Development of Injection Methods (in vitro)

Optimal infusion methods were determined through trial and error *in vitro* prior to implementation *in vivo*. The rate of withdrawal or infusion of each component (oil, air, and virus) was found to be a critical determinant of success for the overall procedure. When withdrawn at a rate higher than the optimum (0.1µL/min), bubbles would form within the oil, preventing a successful infusion. Additionally, due to the viscosity of the oil, higher rates of withdrawal resulted in inaccuracies in the volume of oil collected. Subsequently, if the air was withdrawn at a higher rate, bubbles would form in the oil. Likewise, withdrawing the viral load at higher rates can result in withdrawal of air into the sample and an unsuccessful infusion.

Increased GFAP Expression Surrounding Microfluidic Devices

The inclusion of a microfluidic channel on the device necessarily increases the footprint of the implant. Given evidence for a relationship between device architecture and tissue response (Seymour and Kipke 2007; Kozai et al. 2012), we explored the level of astrogliosis surrounding microfluidic devices in comparison to “traditional” single shank, silicon probes. Microfluidic devices created larger injuries compared to traditional devices, with average injury areas of 0.056mm^2 and 0.004mm^2 respectively (Figure 2.2A). Although the width of the microfluidic device is 185µm, injury sizes were noticeably larger. Hoechst staining confirmed the absence of cells within the injury area (not shown). This exacerbated injury size could be due to tissue adhered to the device being removed while extracting the brain. This larger injury size is accompanied by increased astrogliosis. Quantification of GFAP fluorescence surrounding microfluidic devices show significantly elevated levels of GFAP expression ($p < 0.05$) up to 130µm of the insertion site boundary (relative to distal bin intensity values). Traditional devices show a slightly more spatially restricted response, with significantly elevated levels of GFAP expression ($p < 0.05$)

detected up to 100μm from the device tract. Furthermore, a trend toward an overall elevation in GFAP expression was detected in microfluidic devices in comparison to traditional devices ($p < 0.1$) (Figure 2.2B). These results indicate that the larger footprint of the microfluidic device could slightly exacerbate reactive astrogliosis.

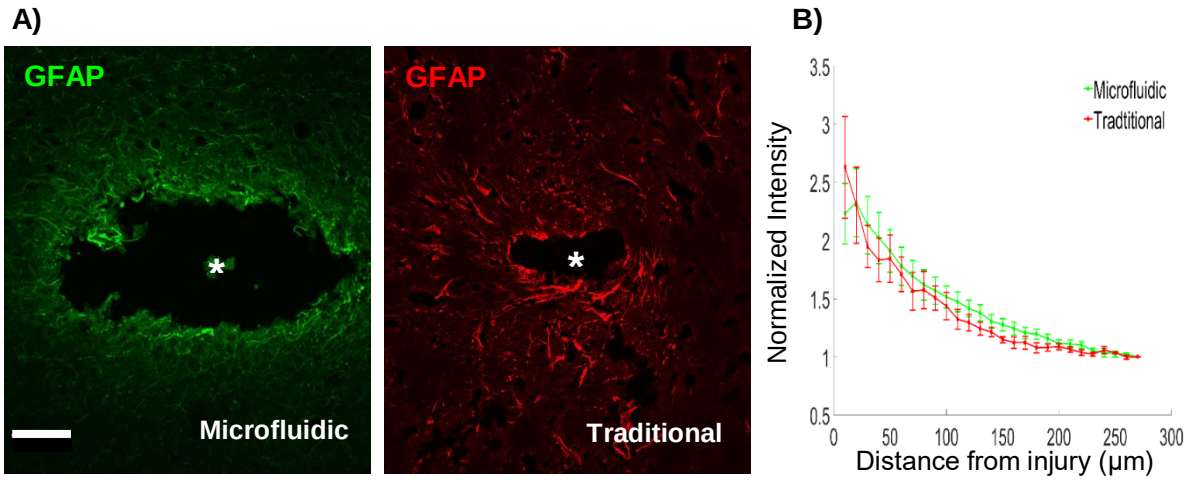

Figure 2.2. Increased GFAP expression surrounding microfluidic devices. A) GFAP staining surrounding microfluidic and traditional devices indicates astrogliosis and a larger injury footprint related to the microfluidic device. Scale bar = 100μm **B)** Microfluidic devices show significantly elevated levels of GFAP expression within 130μm of the injury in comparison to distal control values ($p < 0.05$). Traditional devices have a slightly more compact region of gliosis, with significantly elevated levels of GFAP within 100μm ($p < 0.05$). * denotes injury center.

Signal Quality of Microfluidic Devices

We observed an initial increase in LFP amplitude 1 day post-implantation followed by a gradual decrease in amplitude before stabilizing at 4 weeks post-implantation (Figure 2.3B). These observations follow a general trend of decreasing signal quality over time. Additionally, a cursory observation yielded limited identification of unit activity, with units detected only at 5 days post-implantation (Figure 2.3A). While the sample size is limited, the observation confirms the ability to successfully detect unit activity with the microfluidic devices in a chronic setting.

Microfluidic Devices Successfully Deliver Virus Along the Length of the Injury

Animals were infused 1-3 weeks post-implantation according to the methods developed *in vitro*. Some alterations to the infusion protocol developed *in vitro* were necessary to successfully deliver the viral load *in vivo*. An infusion rate of 0.1μL/min proved insufficient to overcome back

pressure in an *in vivo* setting. Increasing the infusion rate to 0.2μL/min was sufficient for most animals; however, variations between animals required infusion rates up to 0.4μL/min for successful virus delivery.

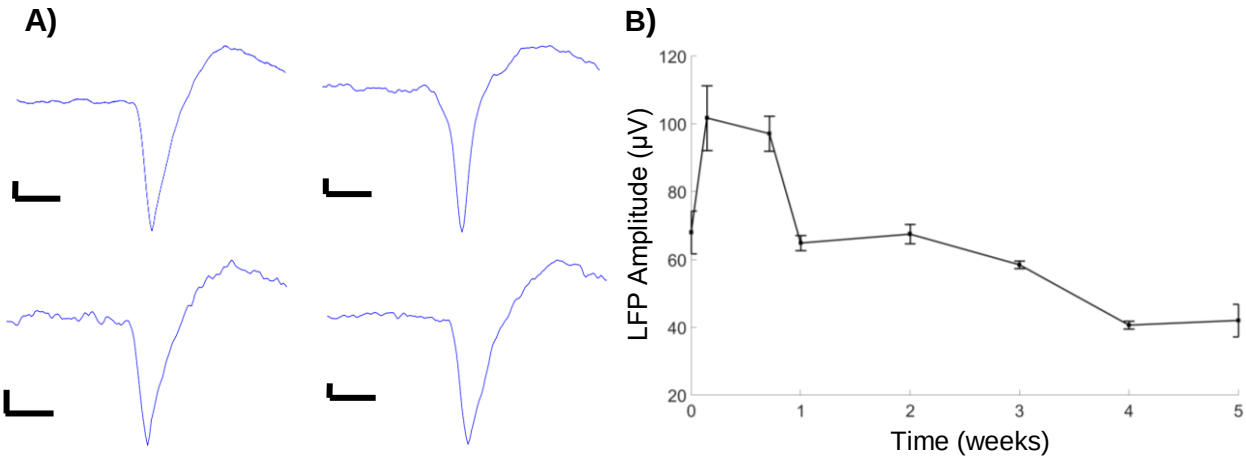

Figure 2.3. Extracellular recordings. A) Recorded units. All scale bars are 10μV amplitude, 0.5msec timescale. **B)** Average LFP amplitude (with error bars) recorded from time of implantation till time of sacrifice.

Animals were sacrificed 2-3 weeks after infusing, and cryosections were imaged with an Olympus Fluoview 1000 confocal microscope to assess expression of the infused virus. All successfully infused animals showed expression of the delivered fluorescent reporter or siRNA construct surrounding the injury site (Figure 2.4). We observed a qualitative increase in the amount of expression and diffusion of the vector at deeper sections of the injury compared to superficial sections. This pattern of dispersion is most likely due to the channel having a single opening at the tip of the probe.

Discussion

While it is widely believed that the biological response to implanted electrodes is intimately linked to their function(Jorfi et al. 2015; Kozai et al. 2015b), direct evidence for this relationship is surprisingly scarce. Multiple studies have explored correlations between a specific measure of

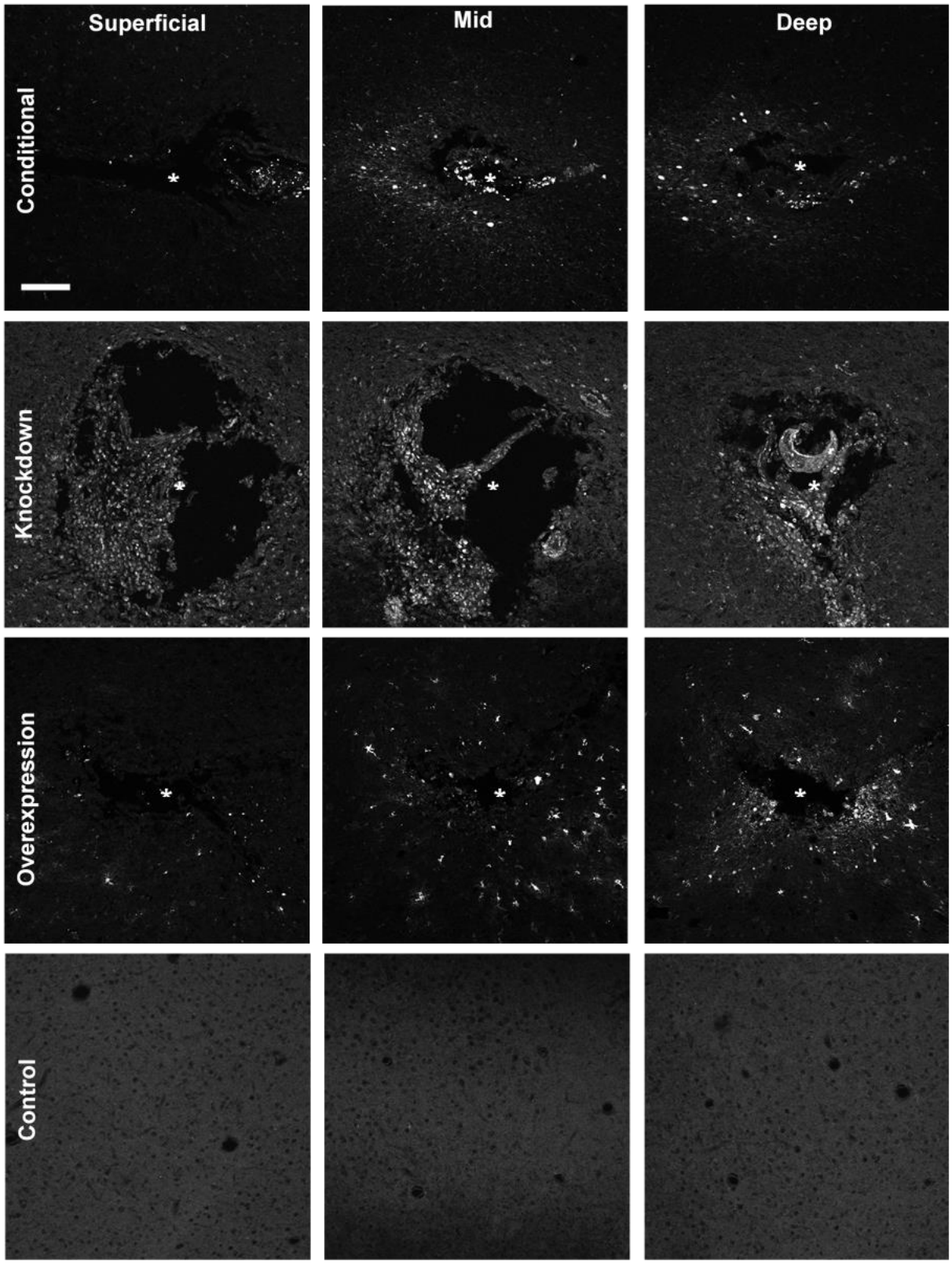

Figure 2.4. Vector expression surrounding microfluidic devices. Spread of fluorescent reporter or siRNA construct expression (appears white) of AAV8-GFAP-mCherry

Figure 2.4. (cont'd) (overexpression), BLOCK-iT™ siRNA (knockdown), and AAV2-Cre-GFP (conditional) at superficial (~100-650μm), mid (~750-1000μm), and deep (~1100-1300μm) sections of the injury. Reporter expression is spatially broader in deep sections of the injury (near the infusion tip) in comparison to more superficial sections. Control images were taken from the contralateral hemisphere * denotes injury center. Scale bar = 100μm

recording quality (such as number of units detected), impedance data, and/or an isolated metric of the biological response (for instance, local neuronal density) to gain insight into the association between functional characteristics and cellular responses. However, the variability in the outcomes reported in these studies underscores the complexity of the multifaceted nature of the underlying source(s) of recorded signal loss, interface instability, and shifting stimulation thresholds(Kozai et al. 2015a; Malaga et al. 2016; Michelson et al. 2018). Likewise, while new device designs incorporate increasingly sophisticated features and materials(Wellman et al. 2018), the relationship between each of these design features, the impacts on tissue response, and chronic device performance remain poorly characterized. The development of new tools and test beds to understand the basic science governing tissue-device interactions could provide a direct link between biological mechanisms and device function, ultimately delivering guiding principles for the design features necessary to enable improved tissue integration.

In the current study, we developed and validated methods to modify gene expression using multiple techniques (silencing, conditional expression, and overexpression). Each of these approaches provides a new "knob" to turn to tune the biological response to devices in controlled ways, potentially providing a mechanistic link between observations of localized changes in gene and/or protein expression and device performance. This approach builds on previous work that has used drug-based strategies to modulate the biological response to electrodes, either through exacerbation or mitigation of effects, to explore the role of neuroinflammation in signal loss. For example, microelectrodes in animals administered lipopolysaccharide, a common pro-inflammatory stimulus, had a notably lower signal-to-noise ratio and fewer units detected compared to control rats, whereas anti-inflammatory drugs have

been shown to decrease neuroinflammation and improve recording quality(Rennaker et al. 2007; Potter et al. 2013; Jorfi et al. 2015; Kozai et al. 2016; Golabchi et al. 2018). However, targeting specific signaling pathways through perturbation of gene expression may offer a more granular view of the key biological mechanisms mediating the neurotoxicity and inflammation that occur at the neural-electrode interface.

As more information on the genes differentially expressed at the device interface becomes available, new opportunities to identify relevant candidate pathways will emerge. Recent studies evaluating gene expression surrounding implanted devices noted increased expression of GFAP, TNFα, NOS2, HMGB1, CD14, and numerous members of the IL gene family(Karumbaiah et al. 2013; Bennett et al. 2018; Ereifej et al. 2018). Additionally, Bennett *et al*. showed genes regulating tight junction and adherens junction proteins in blood brain barrier were downregulated after 72 hours post implantation(Bennett et al. 2018). Manipulation of gene expression by upregulation or downregulation could reveal potential breakthroughs in improving device function and integration in the brain. Further, Cre-recombinase allows an added layer of control of local gene expression by enabling conditional knockout and genome editing(Nagy 2000).

While the approaches developed in this study were successful in localized modulation of gene expression, several areas for future improvement were identified. The epoxy used to attach the plastic tubing to the probe was brittle and prone to cracking. This resulted in the potential loss of the plastic tubing during the natural exploratory behavior of the subject, ultimately leading to the microfluidic channel becoming damaged. A more flexible epoxy could reduce the likelihood of this issue. Additionally, the proximity of the microfluidic channel to the electrical connector necessitated the use of an adapter in order avoid damaging the channel while recording neural activity. While not affecting our ability to infuse, having a single opening at the tip of the probe resulted in unequal distribution of the delivered virus along the length of the probe. Alternative designs that enable more control over the distribution and location of viral delivery would be

beneficial for applications that seek to perturb the environment at specified sites along the length of the probe.

Recent efforts in neural engineering have accentuated the need for understanding the basic science behind the biological mechanisms at the device interface. Next-generation device design is contingent on identifying these unknown device-tissue interactions. This work provides an approach to interrogate and understand the local environment around an implanted device, enabling new opportunities to investigate the tissue response to implants and identify improved device designs.

Author Contributions

Conceptualization, E.P.; Methodology, B.W.; Formal Analysis, B.W.; Investigation, B.W., S.D., J.S..; Writing-Original Draft Preparation, B.W., S.D., E.P.; Writing-Review & Editing, B.W., S.D., J.S., E.P.; Visualization, B.W.; Supervision, E.P.

Funding

This research was supported by the Department of Biomedical Engineering and the Department of Electrical and Computer Engineering at Michigan State University.

Acknowledgments

The authors thank Melinda K. Frame from Center for Advanced Microscopy for confocal training, and Takashi D. Y. Kozai and Zhannetta Gugel for the intensity profiling MATLAB script.

Conflicts of Interest

The authors declare no conflict of interest.

BIBLIOGRAPHY

BIBLIOGRAPHY

Adelman G, **Rane SG**, **Villa KF**. The cost burden of multiple sclerosis in the United States: a systematic review of the literature. *J Med Econ* 16: 639–647, 2013.

Anderson MA, **Ao Y**, **Sofroniew M V.** Heterogeneity of reactive astrocytes. *Neurosci Lett* 565: 23–29, 2014.

Anikeeva P, **Andalman AS**, **Witten I**, **Warden M**, **Goshen I**, **Grosenick L**, **Gunaydin LA**, **Frank LM**, **Deisseroth K**. Optetrode: a multichannel readout for optogenetic control in freely moving mice. *Nat Neurosci* 15: 163–70, 2011.

Arthur KC, **Calvo A**, **Price TR**, **Geiger JT**, **Chiò A**, **Traynor BJ**. Projected increase in amyotrophic lateral sclerosis from 2015 to 2040. *Nat Commun* 7: 12408, 2016.

Bedell HW, **Hermann JK**, **Ravikumar M**, **Lin S**, **Rein A**, **Li X**, **Molinich E**, **Smith PD**, **Selkirk SM**, **Miller RH**, **Sidik S**, **Taylor DM**, **Capadona JR**. Targeting CD14 on blood derived cells improves intracortical microelectrode performance. *Biomaterials* 163: 163–173, 2018.

Benabid AL, **Chabardes S**, **Torres N**, **Piallat B**, **Krack P**, **Fraix V**, **Pollak P**. Functional neurosurgery for movement disorders: a historical perspective. *Prog. Brain Res.* 175: 379–391, 2009.

Bennett C, **Samikkannu M**, **Mohammed F**, **Dietrich WD**, **Rajguru SM**, **Prasad A**. Blood brain barrier (BBB)-disruption in intracortical silicon microelectrode implants. *Biomaterials* 164: 1–10, 2018.

Biran R, **Martin DC**, **Tresco PA**. Neuronal cell loss accompanies the brain tissue response to chronically implanted silicon microelectrode arrays. *Exp Neurol* 195: 115–126, 2005.

Bouton CE, **Shaikhouni A**, **Annetta N V.**, **Bockbrader MA**, **Friedenberg DA**, **Nielson DM**, **Sharma G**, **Sederberg PB**, **Glenn BC**, **Mysiw WJ**, **Morgan AG**, **Deogaonkar M**, **Rezai AR**. Restoring cortical control of functional movement in a human with quadriplegia. *Nature* 533: 247–250, 2016.

Buffo A, **Rolando C**, **Ceruti S**. Astrocytes in the damaged brain: Molecular and cellular insights into their reactive response and healing potential. *Biochem Pharmacol* 79: 77–89, 2010.

Campbell A, **Wu C**, **Campbell A**, **Wu C**. Chronically Implanted Intracranial Electrodes: Tissue Reaction and Electrical Changes. *Micromachines* 9: 430, 2018.

Canales A, **Jia X**, **Froriep UP**, **Koppes RA**, **Tringides CM**, **Selvidge J**, **Lu C**, **Hou C**, **Wei L**, **Fink Y**, **Anikeeva P**. Multifunctional fibers for simultaneous optical, electrical and chemical interrogation of neural circuits in vivo. *Nat Biotechnol* 33: 277–284, 2015.

Cardin JA, **Carlén M**, **Meletis K**, **Knoblich U**, **Zhang F**, **Deisseroth K**, **Tsai L-H**, **Moore CI**. Targeted optogenetic stimulation and recording of neurons in vivo using cell-type-specific expression of Channelrhodopsin-2. *Nat Protoc* 5: 247–254, 2010.

Cavaglia M, **Dombrowski SM**, **Drazba J**, **Vasanji A**, **Bokesch PM**, **Janigro D**. Regional variation in brain capillary density and vascular response to ischemia. *Brain Res* 910: 81–93, 2001.

Chen R, **Canales A**, **Anikeeva P**. Neural recording and modulation technologies. *Nat Rev Mater* 2: 16093, 2017.

Chen Y, **Swanson RA**. Astrocytes and Brain Injury. *J Cereb Blood Flow Metab* 23: 137–149, 2003.

Chen Z-J, **Gillies GT**, **Broaddus WC**, **Prabhu SS**, **Fillmore H**, **Mitchell RM**, **Corwin FD**, **Fatouros PP**. A realistic brain tissue phantom for intraparenchymal infusion studies. *J Neurosurg* 101: 314–322, 2004.

Collinger JL, **Wodlinger B**, **Downey JE**, **Wang W**, **Tyler-Kabara EC**, **Weber DJ**, **McMorland AJ**, **Velliste M**, **Boninger ML**, **Schwartz AB**. High-performance neuroprosthetic control by an individual with tetraplegia. *Lancet* 381: 557–564, 2013.

Dorsey ER, **Constantinescu R**, **Thompson JP**, **Biglan KM**, **Holloway RG**, **Kieburtz K**, **Marshall FJ**, **Ravina BM**, **Schifitto G**, **Siderowf A**, **Tanner CM**. Projected number of people with Parkinson disease in the most populous nations, 2005 through 2030. *Neurology* 68: 384–386, 2007.

Downen M, **Amaral TD**, **Hua LL**, **Zhao M-L**, **Lee SC**. Neuronal death in cytokine-activated primary human brain cell culture: role of tumor necrosis factor-? *Glia* 28: 114–127, 1999.

Eles JR, **Vazquez AL**, **Kozai TDY**, **Cui XT**. In vivo imaging of neuronal calcium during electrode implantation: Spatial and temporal mapping of damage and recovery. *Biomaterials* 174: 79–94, 2018.

Ereifej ES, **Smith CS**, **Meade SM**, **Chen K**, **Feng H**, **Capadona JR**. The Neuroinflammatory Response to Nanopatterning Parallel Grooves into the Surface Structure of Intracortical Microelectrodes. *Adv Funct Mater* 28: 1704420, 2018.

Ezzyat Y, **Wanda PA**, **Levy DF**, **Kadel A**, **Aka A**, **Pedisich I**, **Sperling MR**, **Sharan AD**, **Lega BC**, **Burks A**, **Gross RE**, **Inman CS**, **Jobst BC**, **Gorenstein MA**, **Davis KA**, **Worrell GA**, **Kucewicz MT**, **Stein JM**, **Gorniak R**, **Das SR**, **Rizzuto DS**, **Kahana MJ**. Closed-loop stimulation of temporal cortex rescues functional networks and improves memory. *Nat Commun* 9: 365, 2018.

Golabchi A, **Wu B**, **Li X**, **Carlisle DL**, **Kozai TDY**, **Friedlander RM**, **Cui XT**. Melatonin improves quality and longevity of chronic neural recording. *Biomaterials* 180: 225–239, 2018.

Greenberg PE, **Kessler RC**, **Birnbaum HG**, **Leong SA**, **Lowe SW**, **Berglund PAA**, **Corey-Lisle PK**. The Economic Burden of Depression in the United States: How Did It Change Between 1990 and 2000? *J Clin Psychiatry* 64: 1465–1475, 2003.

Guo Z, **Zhang L**, **Wu Z**, **Chen Y**, **Wang F**, **Chen G**. In Vivo Direct Reprogramming of Reactive Glial Cells into Functional Neurons after Brain Injury and in an Alzheimer's Disease Model. *Cell Stem Cell* 14: 188–202, 2014.

Halpern CH, **Samadani U**, **Litt B**, **Jaggi JL**, **Baltuch GH**. Deep Brain Stimulation for Epilepsy. In: *Neuromodulation*. Elsevier, p. 639–649.

Hascup KN, **Hascup ER**, **Stephens ML**, **Glaser PEA**, **Yoshitake T**, **Mathé AA**, **Gerhardt GA**, **Kehr J**. Resting glutamate levels and rapid glutamate transients in the prefrontal cortex of the Flinders Sensitive Line rat: a genetic rodent model of depression. *Neuropsychopharmacology* 36: 1769–77, 2011.

He W, **Bellamkonda R V.** A Molecular Perspective on Understanding and Modulating the Performance of Chronic Central Nervous System (CNS) Recording Electrodes [Online]. CRC Press/Taylor & Francis. http://www.ncbi.nlm.nih.gov/pubmed/21204400 [31 Oct. 2018].

Heinrich C, **Blum R**, **Gascón S**, **Masserdotti G**, **Tripathi P**, **Sánchez R**, **Tiedt S**, **Schroeder T**, **Götz M**, **Berninger B**. Directing Astroglia from the Cerebral Cortex into Subtype Specific Functional Neurons. *PLoS Biol* 8: e1000373, 2010.

Igarashi H, **Koizumi K**, **Kaneko R**, **Ikeda K**, **Egawa R**, **Yanagawa Y**, **Muramatsu S**, **Onimaru H**, **Ishizuka T**, **Yawo H**. A Novel Reporter Rat Strain That Conditionally Expresses the Bright Red Fluorescent Protein tdTomato. *PLoS One* 11: e0155687, 2016.

Jennings JH, **Stuber GD**. Tools for Resolving Functional Activity and Connectivity within Intact Neural Circuits. *Curr Biol* 24: R41–R50, 2014.

Jeong J-W, **McCall JG**, **Shin G**, **Zhang Y**, **Al-Hasani R**, **Kim M**, **Li S**, **Sim JY**, **Jang K-I**, **Shi Y**, **Hong DY**, **Liu Y**, **Schmitz GP**, **Xia L**, **He Z**, **Gamble P**, **Ray WZ**, **Huang Y**, **Bruchas MR**, **Rogers JA**. Wireless Optofluidic Systems for Programmable In Vivo Pharmacology and Optogenetics. *Cell* 162: 662–674, 2015.

Jorfi M, **Skousen JL**, **Weder C**, **Capadona JR**. Progress towards biocompatible intracortical microelectrodes for neural interfacing applications. *J Neural Eng* 12: 011001, 2015.

Karumbaiah L, **Saxena T**, **Carlson D**, **Patil K**, **Patkar R**, **Gaupp EA**, **Betancur M**, **Stanley GB**, **Carin L**, **Bellamkonda R V.** Relationship between intracortical electrode design and chronic recording function. *Biomaterials* 34: 8061–8074, 2013.

Khan W, **Li W**. Wafer level fabrication method of hemispherical reflector coupled micro-led array stimulator for optogenetics. In: *2017 19th International Conference on Solid-State Sensors, Actuators and Microsystems (TRANSDUCERS)*. IEEE, p. 2231–2234.

Konermann S, **Brigham MD**, **Trevino A**, **Hsu PD**, **Heidenreich M**, **Cong L**, **Platt RJ**, **Scott DA**, **Church GM**, **Zhang F**. Optical control of mammalian endogenous transcription and epigenetic states. *Nature* 500: 472–476, 2013.

Kowal SL, **Dall TM**, **Chakrabarti R**, **Storm M V.**, **Jain A**. The current and projected economic burden of Parkinson's disease in the United States. *Mov Disord* 28: 311–318, 2013.

Kozai TDY, **Catt K**, **Li X**, **Gugel Z V.**, **Olafsson VT**, **Vazquez AL**, **Cui XT**. Mechanical failure modes of chronically implanted planar silicon-based neural probes for laminar recording. *Biomaterials* 37: 25–39, 2015a.

Kozai TDY, **Gugel Z**, **Li X**, **Gilgunn PJ**, **Khilwani R**, **Ozdoganlar OB**, **Fedder GK**, **Weber DJ**,

Cui XT. Chronic tissue response to carboxymethyl cellulose based dissolvable insertion needle for ultra-small neural probes. *Biomaterials* 35: 9255–9268, 2014.

Kozai TDY, **Jaquins-Gerstl AS**, **Vazquez AL**, **Michael AC**, **Cui XT**. Brain tissue responses to neural implants impact signal sensitivity and intervention strategies. *ACS Chem Neurosci* 6: 48–67, 2015b.

Kozai TDY, **Jaquins-Gerstl AS**, **Vazquez AL**, **Michael AC**, **Cui XT**. Dexamethasone retrodialysis attenuates microglial response to implanted probes in vivo. *Biomaterials* 87: 157–169, 2016.

Kozai TDY, **Langhals NB**, **Patel PR**, **Deng X**, **Zhang H**, **Smith KL**, **Lahann J**, **Kotov NA**, **Kipke DR**. Ultrasmall implantable composite microelectrodes with bioactive surfaces for chronic neural interfaces. *Nat Mater* 11: 1065–1073, 2012.

Lebedev MA, **Nicolelis MAL**. Brain–machine interfaces: past, present and future. *Trends Neurosci* 29: 536–546, 2006.

Lee M, **Schwab C**, **Mcgeer PL**. Astrocytes are GABAergic cells that modulate microglial activity. *Glia* 59: 152–165, 2011.

Liddelow SA, **Guttenplan KA**, **Clarke LE**, **Bennett FC**, **Bohlen CJ**, **Schirmer L**, **Bennett ML**, **Münch AE**, **Chung W-S**, **Peterson TC**, **Wilton DK**, **Frouin A**, **Napier BA**, **Panicker N**, **Kumar M**, **Buckwalter MS**, **Rowitch DH**, **Dawson VL**, **Dawson TM**, **Stevens B**, **Barres BA**. Neurotoxic reactive astrocytes are induced by activated microglia. *Nature* 541: 481–487, 2017.

Ludwig K a, **Uram JD**, **Yang J**, **Martin DC**, **Kipke DR**. Chronic neural recordings using silicon microelectrode arrays electrochemically deposited with a poly(3,4-ethylenedioxythiophene) (PEDOT) film. *J Neural Eng* 3: 59–70, 2006.

Ludwig KA, **Miriani RM**, **Langhals NB**, **Joseph MD**, **Anderson DJ**, **Kipke DR**. Using a Common Average Reference to Improve Cortical Neuron Recordings From Microelectrode Arrays. *J Neurophysiol* 101: 1679–1689, 2009.

Malaga KA, **Schroeder KE**, **Patel PR**, **Irwin ZT**, **Thompson DE**, **Bentley JN**, **Lempka SF**, **Chestek CA**, **Patil PG**. Data-driven model comparing the effects of glial scarring and interface interactions on chronic neural recordings in non-human primates. *J Neural Eng J Neural Eng* 13: 16010–16024, 2016.

Malone DA, **Dougherty DD**, **Rezai AR**, **Carpenter LL**, **Friehs GM**, **Eskandar EN**, **Rauch SL**, **Rasmussen SA**, **Machado AG**, **Kubu CS**, **Tyrka AR**, **Price LH**, **Stypulkowski PH**, **Giftakis JE**, **Rise MT**, **Malloy PF**, **Salloway SP**, **Greenberg BD**. Deep Brain Stimulation of the Ventral Capsule/Ventral Striatum for Treatment-Resistant Depression. *Biol Psychiatry* 65: 267–275, 2009.

Mayberg HS, **Lozano AM**, **Voon V**, **McNeely HE**, **Seminowicz D**, **Hamani C**, **Schwalb JM**, **Kennedy SH**. Deep Brain Stimulation for Treatment-Resistant Depression. *Neuron* 45: 651–660, 2005.

McCreery D, **Cogan S**, **Kane S**, **Pikov V**. Correlations between histology and neuronal activity recorded by microelectrodes implanted chronically in the cerebral cortex. *J Neural Eng* 13:

036012, 2016.

Michelson NJ, **Vazquez AL**, **Eles JR**, **Salatino JW**, **Purcell EK**, **Williams JJ**, **Cui XT**, **Kozai TDY**. Multi-scale, multi-modal analysis uncovers complex relationship at the brain tissue-implant neural interface: new emphasis on the biological interface. *J Neural Eng* 15: 033001, 2018.

Motta-Mena LB, **Reade A**, **Mallory MJ**, **Glantz S**, **Weiner OD**, **Lynch KW**, **Gardner KH**. An optogenetic gene expression system with rapid activation and deactivation kinetics. *Nat Chem Biol* 10: 196–202, 2014.

Nagy A. Cre recombinase: The universal reagent for genome tailoring. *genesis* 26: 99–109, 2000.

Nolta NF, **Christensen MB**, **Crane PD**, **Skousen JL**, **Tresco PA**. BBB leakage, astrogliosis, and tissue loss correlate with silicon microelectrode array recording performance. *Biomaterials* 53: 753–762, 2015.

O'Doherty JE, **Lebedev MA**, **Ifft PJ**, **Zhuang KZ**, **Shokur S**, **Bleuler H**, **Nicolelis MAL**. Active tactile exploration using a brain-machine-brain interface. *Nature* 479: 228–31, 2011.

Oakes RS, **Polei MD**, **Skousen JL**, **Tresco PA**. An astrocyte derived extracellular matrix coating reduces astrogliosis surrounding chronically implanted microelectrode arrays in rat cortex. *Biomaterials* 154: 1–11, 2018.

Perry VH, **Teeling J**. Microglia and macrophages of the central nervous system: the contribution of microglia priming and systemic inflammation to chronic neurodegeneration. *Semin Immunopathol* 35: 601–12, 2013.

Polikov VS, **Tresco PA**, **Reichert WM**. Response of brain tissue to chronically implanted neural electrodes. *J Neurosci Methods* 148: 1–18, 2005.

Potter KA, **Buck AC**, **Self WK**, **Callanan ME**, **Sunil S**, **Capadona JR**. The effect of resveratrol on neurodegeneration and blood brain barrier stability surrounding intracortical microelectrodes. *Biomaterials* 34: 7001–7015, 2013.

Purcell EK, **Thompson DE**, **Ludwig KA**, **Kipke DR**. Flavopiridol reduces the impedance of neural prostheses in vivo without affecting recording quality. *J Neurosci Methods* 183: 149–157, 2009.

Purcell EK, **Yang A**, **Liu L**, **Velkey JM**, **Morales MM**, **Duncan RK**. BDNF profoundly and specifically increases KCNQ4 expression in neurons derived from embryonic stem cells. *Stem Cell Res* 10: 29–35, 2013.

Ralay Ranaivo H, **Wainwright MS**. Albumin activates astrocytes and microglia through mitogen-activated protein kinase pathways. *Brain Res* 1313: 222–31, 2010.

Rennaker RL, **Miller J**, **Tang H**, **Wilson DA**. Minocycline increases quality and longevity of chronic neural recordings. *J Neural Eng* 4: L1-5, 2007.

Rosin B, **Slovik M**, **Mitelman R**, **Rivlin-Etzion M**, **Haber SN**, **Israel Z**, **Vaadia E**, **Bergman H**. Closed-Loop Deep Brain Stimulation Is Superior in Ameliorating Parkinsonism. *Neuron* 72: 370–

384, 2011.

Rossi JL, **Ralay Ranaivo H**, **Patel F**, **Chrzaszcz M**, **Venkatesan C**, **Wainwright MS**. Albumin causes increased myosin light chain kinase expression in astrocytes via p38 mitogen-activated protein kinase. *J Neurosci Res* 89: 852–61, 2011.

Salatino JW, **Ludwig KA**, **Kozai TDY**, **Purcell EK**. Glial responses to implanted electrodes in the brain. *Nat Biomed Eng* 1: 862–877, 2017a.

Salatino JW, **Winter BM**, **Drazin MH**, **Purcell EK**. Functional remodeling of subtype-specific markers surrounding implanted neuroprostheses. *J Neurophysiol* 118: 194–202, 2017b.

Seidl K, **Spieth S**, **Herwik S**, **Steigert J**, **Zengerle R**, **Paul O**, **Ruther P**. In-plane silicon probes for simultaneous neural recording and drug delivery. *J Micromechanics Microengineering* 20: 105006, 2010.

Seymour JP, **Kipke DR**. Neural probe design for reduced tissue encapsulation in CNS. *Biomaterials* 28: 3594–3607, 2007.

Shen Q, **Rigor RR**, **Pivetti CD**, **Wu MH**, **Yuan SY**. Myosin light chain kinase in microvascular endothelial barrier function. *Cardiovasc Res* 87: 272–80, 2010.

Shen W, **Karumbaiah L**, **Liu X**, **Saxena T**, **Chen S**, **Patkar R**, **Bellamkonda R V.**, **Allen MG**. Extracellular matrix-based intracortical microelectrodes: Toward a microfabricated neural interface based on natural materials. *Microsystems Nanoeng* 1: 15010, 2015.

Sofroniew M V. Molecular dissection of reactive astrogliosis and glial scar formation. *Trends Neurosci* 32: 638–47, 2009.

Sofroniew M V. Astrogliosis. *Cold Spring Harb Perspect Biol* 7: a020420, 2014.

Sofroniew M V, **Vinters H V**. Astrocytes: biology and pathology. *Acta Neuropathol* 119: 7–35, 2010.

Sommakia S, **Lee HC**, **Gaire J**, **Otto KJ**. Materials approaches for modulating neural tissue responses to implanted microelectrodes through mechanical and biochemical means. *Curr Opin Solid State Mater Sci* 18: 319–328, 2014.

Suo Z, **Wu M**, **Citron BA**, **Gao C**, **Festoff BW**. Persistent protease-activated receptor 4 signaling mediates thrombin-induced microglial activation. *J Biol Chem* 278: 31177–83, 2003.

Tong M, **Hernandez JL**, **Purcell EK**, **Altschuler RA**, **Duncan RK**. The intrinsic electrophysiological properties of neurons derived from mouse embryonic stem cells overexpressing neurogenin-1. *Am J Physiol Physiol* 299: C1335–C1344, 2010.

Vierbuchen T, **Ostermeier A**, **Pang ZP**, **Kokubu Y**, **Südhof TC**, **Wernig M**. Direct conversion of fibroblasts to functional neurons by defined factors. *Nature* 463: 1035–1041, 2010.

Volterra A, **Meldolesi J**. Astrocytes, from brain glue to communication elements: the revolution continues. *Nat Rev Neurosci* 6: 626–640, 2005.

Weaver FM, **Follett K**, **Stern M**, **Hur K**, **Harris C**, **Marks WJ**, **Rothlind J**, **Sagher O**, **Reda D**, **Moy CS**, **Pahwa R**, **Burchiel K**, **Hogarth P**, **Lai EC**, **Duda JE**, **Holloway K**, **Samii A**, **Horn S**, **Bronstein J**, **Stoner G**, **Heemskerk J**, **Huang GD**, **Group for the C 468 S**, **KA F**, **S M**, **J C**, **RL R**, **F W**, **AE L**, **Y T**, **P K**, **G D**, **MM H**, **JW L**, **MF F**, **S F**, **RS S**, **V P**, **RA H**, **CG G**, **R P**, **A S**, **K S-T**, **H J**, **P L**, **K W**, **M A**, **BS A**, **Y T**, **KJ B**, **MI H**. Bilateral Deep Brain Stimulation vs Best Medical Therapy for Patients With Advanced Parkinson Disease<subtitle>A Randomized Controlled Trial</subtitle> *JAMA* 301: 63, 2009.

Weinstein JR, **Gold SJ**, **Cunningham DD**, **Gall CM**, **Sastre A**, **Lyuboslavsky P**, **Hepler JR**, **McKeon RJ**, **Traynelis SF**. Cellular localization of thrombin receptor mRNA in rat brain: expression by mesencephalic dopaminergic neurons and codistribution with prothrombin mRNA. *J Neurosci* 15: 2906–19, 1995.

Wellman SM, **Eles JR**, **Ludwig KA**, **Seymour JP**, **Michelson NJ**, **McFadden WE**, **Vazquez AL**, **Kozai TDY**. A Materials Roadmap to Functional Neural Interface Design. *Adv Funct Mater* 28: 1701269, 2018.

Wimo A, **Jönsson L**, **Bond J**, **Prince M**, **Winblad B**, **Alzheimer Disease International**. The worldwide economic impact of dementia 2010. *Alzheimers Dement* 9: 1–11.e3, 2013.

Winter B, **Daniels S**, **Salatino J**, **Purcell E**. Genetic Modulation at the Neural Microelectrode Interface: Methods and Applications. *Micromachines 2018, Vol 9, Page 476* 9: 476, 2018.

Winter BM, **Setien MB**, **Salatino JW**, **Blanke N**, **Thompson CH**, **Smith KR**, **Khan WA**, **Li W**, **Suhr ST**, **Purcell EK**. Control of cell fate and excitability at the neural electrode interface: Genetic reprogramming and optical induction. In: *2017 IEEE Life Sciences Conference (LSC)*. IEEE, p. 157–161.

Zamanian JL, **Xu L**, **Foo LC**, **Nouri N**, **Zhou L**, **Giffard RG**, **Barres BA**. Genomic analysis of reactive astrogliosis. *J Neurosci* 32: 6391–410, 2012.

CHAPTER 3 An in vitro model of a reactive subtype of astrocyte

Introduction

Astrocytes play multiple supportive roles in the central nervous system (CNS) that are crucial for maintaining normal function. Astrocytes regulate the blood-brain barrier (BBB), maintain homeostasis in the extracellular environment, and glutamate uptake. Additionally, as the third member of the tripartite synapse, astrocytes directly modulate synaptic activity through the release of gliotransmitters (glutamate, D-serine, adenosine triphosphate (ATP))(Volterra and Meldolesi 2005; Salatino et al. 2017a; Campbell et al. 2018). Upon injury, astrocytes become activated and enter a reactive state characterized by cellular hypertrophy, increased proliferation, and upregulation of glial fibrillary acidic protein (GFAP)(Sofroniew and Vinters 2010). Reactive astrocytes produce cytokines, small proteins that act as molecular mediators for intercellular communication, which cause a cascading effect that lead to further damage and astrocyte activation(He and Bellamkonda 2008; Campbell et al. 2018).

However, this reactive state is not homogeneous, but rather exists on a gradient ranging from reversible hypertrophy and alterations in gene expression to compact glial scar formation, depending on the distance from the injury site(Sofroniew 2009). Furthermore, ablation of reactive astrocytes results in increased tissue damage, failure to repair damage to the BBB and increased neuronal loss and demyelination, indicating that astrogliosis has neuroprotective qualities and is not unilaterally negative(Sofroniew 2009). These variations in astrocytic response to injury suggest possible unique reactive astrocyte subtypes.

Activation of astrocytes due to insults causes upregulation of a variety of genes(Sofroniew 2014). Given recent advances identifying unique reactive astrocyte subtypes in stroke injuries and lipopolysaccharide induced neuroinflammation, it seems plausible that novel reactive astrocyte subtypes exist surrounding implanted MEAs(Zamanian et al. 2012). Here, I explore the induction of reactive astrocyte subtypes due to electrode implantation. Based on research

by Liddelow and colleagues, we first tried to create an in vitro model of reactive astrocytes. Rat cortical astrocytes were cultured in serum free media before being exposed to tumor necrosis factor α (TNFα), complement component 1 subcomponent q (C1q), and interleukin 1 α (IL-1α), inducing the neurotoxic “A1” reactive astrocyte subtype, characterized by elevated complement component 3 subcomponent d expression (C3d)(Liddelow et al. 2017). In addition, I investigate means of mediating astrocyte activation using γ-aminobutyric acid (GABA)(Lee et al. 2011).

Methods

Astrocyte culture and cytokine exposure

Rat cortical astrocytes (N7745100 ThermoFisher) were thawed and expanded according to manufacturer specifications. Once 100% confluency was reached, astrocytes were cultured for seven days in serum free media (50mL Neurobasal Media (21103049 ThermoFisher), 125µL GlutaMAX Supplement (35050061 ThermoFisher), 1mL B-27 Supplement (50x) (17504044 ThermoFisher)). Cytokines and GABA were first reconstituted according to manufacturer specifications into 1000x concentrated solutions (30µg/mL TNFα in sterile phosphate buffered saline (PBS) (D8527, Sigma-Aldrich), 3µg/mL Il-1α in distilled deionized H20 (DD H20), 400µg/mL C1q in DDH20, 30mM GABA in DD H20). Cytokine and GABA solutions were diluted to the desired concentrations in serum free media (30ng/mL TNFα, 400ng/mL C1q, 3ng/mL IL-1α, 30µM GABA) before being applied to astrocytes for 24 hours.

Immunocytochemistry

Cells were fixed with 4% paraformaldehyde (PFA) for 15 minutes followed by three 10 minute rinses of PBS. Cells were blocked in 10% normal goat serum (NGS) in PBS for one hour. Subsequently, cells were incubated overnight at 4°C with mouse anti-glial fibrillary acidic protein (GFAP) (1:500, 3670S Cell Signaling Technology) and rabbit anti-C3d (ab136916 Abcam). The following day, cells were rinsed with PBS and incubated with goat anti-mouse IgG (H+L) Alexa Fluor 488 conjugate (1:200, A-1101 ThermoFisher) and goat anti-rabbit IgG (H+L) Alexa Fluor 594 conjugate (1:200, A-11037 ThermoFisher) for two hours at room temperature. Nuclei were

counterstained with Hoechst before cells were stored in PBS at 4°C. Images were obtained using a Nikon Eclipse TE2000-U inverted microscope or a Nikon A1 Turf microscope.

Surgical Procedure

Adult male Sprague-Dawley rats were unilaterally implanted in the motor cortex with a 16-channel single shank microelectrode array (MEA) with a microfluidic channel (E16-4mm-100-177 NeuroNexus). Animals were anesthetized with ~2% isoflurane for the duration of the procedure. Using a motorized drill, a 2mm x 2mm craniotomy was made to expose the cortex (3mm anterior, 2.5mm lateral to bregma). The dura was resected and the MEA was implanted at a 2mm depth in the cortex. The MEA was supported using a dental acrylic headcap anchored by three bone screws. Bupivacaine was administered for topical analgesia, at the wound site, and meloxicam was administered for systemic analgesia, via an intraperitoneal injection during recovery.

Immunohistochemistry

Three weeks post-implantation, animals were deeply anesthetized with an overdose of sodium pentobarbital, and transcardially perfused with 4% paraformaldehyde (PFA). Brains were extracted, stored in 4% PFA overnight and cryoembedded, following sucrose protection. Cryosections were collected at a 20µm thickness and hydrated with PBS, prior to blocking in a 10% normal goat serum in PBS for 1 h. Tissue was subsequently incubated overnight, at 4 °C, with the mouse anti-GFAP (1:500, 3670S Cell Signaling Technology). The following day, cryosections were rinsed with PBS and incubated with the goat anti-mouse IgG (H+L) Alexa Fluor 488 conjugate (1:200, A-1101 ThermoFisher) and goat anti-rabbit IgG (H+L) Alexa Fluor 594 conjugate (1:200, A-11037 ThermoFisher) for two hours at room temperature. Finally, nuclei were counterstained with Hoechst and coverslipped with ProLong Gold antifade reagent (Fisher Scientific Company). An Olympus Fluoview 1000 inverted confocal microscope was used to image samples with a 20× PlanFluor dry objective (0.5NA).

Image Analysis

Images were analyzed using a modified MATLAB script adapted from Kozai and colleagues(Kozai et al. 2014). For analyzing fluorescence intensity surrounding implanted MEAs, the image is divided into concentric 10μm bins radiating from the injury site. Mean fluorescence intensity is calculated in each bin using 5% of the pixels in the corners of the image as a reference. The calculated intensity in each bin was then normalized to the most distal bin. The previous iteration of the script allowed only for a rectangular bin outline, however, this often resulted in tissue at the interfacial region being excluded from calculation or portions of the injury being included in calculation. To address these concerns, I reprogrammed the script to allow the user to define the injury outline by hand. From this outline, concentric bins are created by calculating a linear line from the center of the injury to each point on the user defined outline and shifting each point along that line. For analyzing fluorescence intensity of cell cultures, the image was not binned. The mean of intensity of the whole image was calculated using the corners as a reference. Intensity was then normalized to the control group. Results were assessed using a mixed model ANOVA and SPSS software (IBM) as previously described(Salatino et al. 2017b).

In addition to changes that altered the script's calculations, several modifications were made to the user interface. The original script, which only allowed for the analysis of a single greyscale image, has been altered to process multiple, full color images, allowing the results of all stains to be grouped by sample rather than processed individually. Analysis settings such as bin width and the microns per pixel are hard coded eliminating the need to re-enter settings for each image. Results are automatically organized by the image filename in a location specified by the user. The overall changes result in fewer user inputs, ultimately streamlining the data analysis process.

Results

In vitro cytokine exposure

Astrocytes were exposed to cytokines (TNFα, C1q, and IL-1α), GABA, or both for 24 hours. Following exposure, cells were stained for GFAP and C3d to assess astrocytic activation and the induction of the A1 neurotoxic reactive astrocyte (Figure 3.1A-B). Quantification of GFAP fluorescence reveals that neither the cytokines nor GABA significantly elevated nor reduced expression. Contrary to previous studies, cytokines alone did not significantly elevate C3d expression levels. Cells exposed to either a combination of cytokines and GABA or GABA alone did exhibit significantly elevated C3d expression ($p<0.05$), however, the cytokines seemed to attenuate the induction of the A1 subtype.

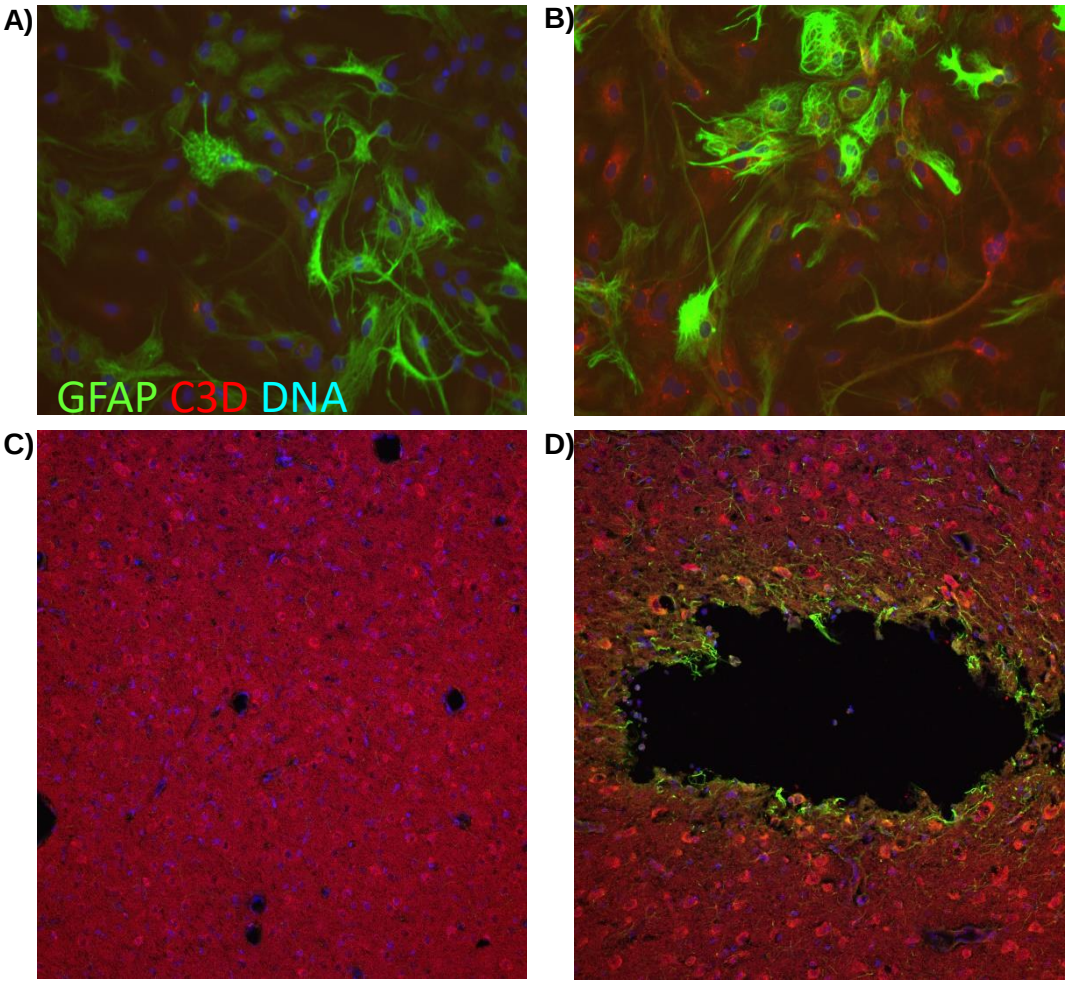

Figure 3.1. C3d expression due to cytokine exposure and electrode implantation. Increased C3d expression **(B)** due to cytokine exposure compared to control conditions **(A)**.

(Figure 3.1 cont'd) Electrode implantation **(D)** induces increased C3d expression compared to contralateral controls **(C)**.

In vivo immunohistochemistry

To verify if the A1 reactive astrocyte is induced in vivo, adult male Sprague-Dawley rats were implanted with MEAs. Three weeks post-implantation, rats were sacrificed and cryosections were stained for GFAP and C3d to evaluate the amount of astrogliosis and identify A1 reactive astrocytes respectively. Sections showed significantly elevated levels of GFAP expression ($p<0.05$) up to 190 µm from the injury boundary. Areas of elevated C3d expression were detected; however, they were not continuous (Figure 3.1C-D). C3d expression was found to be significantly elevated ($p<0.05$) up to 40µm from the injury boundary as well as 70µm and 90µm from the injury boundary. While MEA implantation does induce the neurotoxic A1 astrocyte, induction is not present throughout the area of astrocyte activation.

Future directions

These preliminary results provide a stepping stone to develop a model of reactive astrogliosis surrounding electrode implantation, however, further research is needed to reduce variability and fully explain these observations. Unique subtypes should be identifiable based on distinct gene expression patterns, showing upregulation of distinct and non-overlapping genes. To assess changes in gene expression and identify reactive astrocyte subtypes, we will perform genomic analysis of the reactive astrocyte population at the device-tissue interface. We will model the reactive tissue response *in vitro* to identify conditions under which specific reactive astrocyte states are induced. Additionally, we will assess neurotoxic or neurotrophic effects of the induced reactive states through electrophysiology and immunofluorescence staining. Future experiments include:

Perform genomic analysis of reactive astrocytes surrounding implanted microelectrode arrays and identify reactive astrocyte subtypes based on gene expression.

We will implant an MEA in the motor cortex of rats (M1) to induce reactive gliosis in the surrounding tissue. Given that the glial sheath varies temporally, rats will be sacrificed at one, three, and seven days post implantation. Tissue surrounding the injury will be excised and

reactive astrocytes will be isolated using fluorescence-activated cell sorting (FACS). Upregulated genes will be identified using RNA sequencing (RNA-Seq). We hypothesize that reactive astrocyte subtypes will have unique patterns of gene expression.

Identify conditions under which reactive astrocyte subtypes are induced through in vitro modeling of the reactive tissue response.
Implantation of MEAs punctures cells, releasing ATP and blood serum proteins into the extracellular environment activating microglia. Subsequently, activated microglia release cytokines and other molecules causing a signaling cascade that alters astrocytes and subsequently impairs neuronal health. We will culture astrocytes in serum free media and expose them to combinations of these proteins and molecules. Subsequently, gene expression will be assessed using RNA-Seq.

Assess effects of reactive astrocyte subtypes on neural health and synaptic activity.
Reactive astrocytes will be induced in vitro as described above. Cultured neurons will be exposed to reactive astrocyte conditioned media. At predetermined time points, whole cell patch clamping will be performed on pre- and post-synaptic neurons simultaneously to assess changes in synaptic activity. Additionally, live/dead assays will be performed to determine whether a reactive astrocyte subtype is neurotoxic or neuroprotective.

Conclusions

This thesis explores means of ameliorating the foreign body response and restoring the neuronal population at the device-tissue interface through the delivery of pro-neuronal transcription factors and provides a viable method for perturbing tissue at the interfacial region through targeted vector delivery. It also lays the groundwork for characterizing and modeling a device-reactive subtype of astrocyte. While some of the results presented are preliminary, they offer a stepping stone to more precisely perturb the foreign body response to produce more favorable outcomes.

BIBLIOGRAPHY

BIBLIOGRAPHY

Adelman G, **Rane SG**, **Villa KF**. The cost burden of multiple sclerosis in the United States: a systematic review of the literature. *J Med Econ* 16: 639–647, 2013.

Anderson MA, **Ao Y**, **Sofroniew M V.** Heterogeneity of reactive astrocytes. *Neurosci Lett* 565: 23–29, 2014.

Anikeeva P, **Andalman AS**, **Witten I**, **Warden M**, **Goshen I**, **Grosenick L**, **Gunaydin LA**, **Frank LM**, **Deisseroth K**. Optetrode: a multichannel readout for optogenetic control in freely moving mice. *Nat Neurosci* 15: 163–70, 2011.

Arthur KC, **Calvo A**, **Price TR**, **Geiger JT**, **Chiò A**, **Traynor BJ**. Projected increase in amyotrophic lateral sclerosis from 2015 to 2040. *Nat Commun* 7: 12408, 2016.

Bedell HW, **Hermann JK**, **Ravikumar M**, **Lin S**, **Rein A**, **Li X**, **Molinich E**, **Smith PD**, **Selkirk SM**, **Miller RH**, **Sidik S**, **Taylor DM**, **Capadona JR**. Targeting CD14 on blood derived cells improves intracortical microelectrode performance. *Biomaterials* 163: 163–173, 2018.

Benabid AL, **Chabardes S**, **Torres N**, **Piallat B**, **Krack P**, **Fraix V**, **Pollak P**. Functional neurosurgery for movement disorders: a historical perspective. *Prog. Brain Res.* 175: 379–391, 2009.

Bennett C, **Samikkannu M**, **Mohammed F**, **Dietrich WD**, **Rajguru SM**, **Prasad A**. Blood brain barrier (BBB)-disruption in intracortical silicon microelectrode implants. *Biomaterials* 164: 1–10, 2018.

Biran R, **Martin DC**, **Tresco PA**. Neuronal cell loss accompanies the brain tissue response to chronically implanted silicon microelectrode arrays. *Exp Neurol* 195: 115–126, 2005.

Bouton CE, **Shaikhouni A**, **Annetta N V.**, **Bockbrader MA**, **Friedenberg DA**, **Nielson DM**, **Sharma G**, **Sederberg PB**, **Glenn BC**, **Mysiw WJ**, **Morgan AG**, **Deogaonkar M**, **Rezai AR**. Restoring cortical control of functional movement in a human with quadriplegia. *Nature* 533: 247–250, 2016.

Buffo A, **Rolando C**, **Ceruti S**. Astrocytes in the damaged brain: Molecular and cellular insights into their reactive response and healing potential. *Biochem Pharmacol* 79: 77–89, 2010.

Campbell A, **Wu C**, **Campbell A**, **Wu C**. Chronically Implanted Intracranial Electrodes: Tissue Reaction and Electrical Changes. *Micromachines* 9: 430, 2018.

Canales A, **Jia X**, **Froriep UP**, **Koppes RA**, **Tringides CM**, **Selvidge J**, **Lu C**, **Hou C**, **Wei L**, **Fink Y**, **Anikeeva P**. Multifunctional fibers for simultaneous optical, electrical and chemical interrogation of neural circuits in vivo. *Nat Biotechnol* 33: 277–284, 2015.

Cardin JA, **Carlén M**, **Meletis K**, **Knoblich U**, **Zhang F**, **Deisseroth K**, **Tsai L-H**, **Moore CI**. Targeted optogenetic stimulation and recording of neurons in vivo using cell-type-specific expression of Channelrhodopsin-2. *Nat Protoc* 5: 247–254, 2010.

Cavaglia M, **Dombrowski SM**, **Drazba J**, **Vasanji A**, **Bokesch PM**, **Janigro D**. Regional variation in brain capillary density and vascular response to ischemia. *Brain Res* 910: 81–93, 2001.

Chen R, **Canales A**, **Anikeeva P**. Neural recording and modulation technologies. *Nat Rev Mater* 2: 16093, 2017.

Chen Y, **Swanson RA**. Astrocytes and Brain Injury. *J Cereb Blood Flow Metab* 23: 137–149, 2003.

Chen Z-J, **Gillies GT**, **Broaddus WC**, **Prabhu SS**, **Fillmore H**, **Mitchell RM**, **Corwin FD**, **Fatouros PP**. A realistic brain tissue phantom for intraparenchymal infusion studies. *J Neurosurg* 101: 314–322, 2004.

Collinger JL, **Wodlinger B**, **Downey JE**, **Wang W**, **Tyler-Kabara EC**, **Weber DJ**, **McMorland AJ**, **Velliste M**, **Boninger ML**, **Schwartz AB**. High-performance neuroprosthetic control by an individual with tetraplegia. *Lancet* 381: 557–564, 2013.

Dorsey ER, **Constantinescu R**, **Thompson JP**, **Biglan KM**, **Holloway RG**, **Kieburtz K**, **Marshall FJ**, **Ravina BM**, **Schifitto G**, **Siderowf A**, **Tanner CM**. Projected number of people with Parkinson disease in the most populous nations, 2005 through 2030. *Neurology* 68: 384–386, 2007.

Downen M, **Amaral TD**, **Hua LL**, **Zhao M-L**, **Lee SC**. Neuronal death in cytokine-activated primary human brain cell culture: role of tumor necrosis factor-? *Glia* 28: 114–127, 1999.

Eles JR, **Vazquez AL**, **Kozai TDY**, **Cui XT**. In vivo imaging of neuronal calcium during electrode implantation: Spatial and temporal mapping of damage and recovery. *Biomaterials* 174: 79–94, 2018.

Ereifej ES, **Smith CS**, **Meade SM**, **Chen K**, **Feng H**, **Capadona JR**. The Neuroinflammatory Response to Nanopatterning Parallel Grooves into the Surface Structure of Intracortical Microelectrodes. *Adv Funct Mater* 28: 1704420, 2018.

Ezzyat Y, **Wanda PA**, **Levy DF**, **Kadel A**, **Aka A**, **Pedisich I**, **Sperling MR**, **Sharan AD**, **Lega BC**, **Burks A**, **Gross RE**, **Inman CS**, **Jobst BC**, **Gorenstein MA**, **Davis KA**, **Worrell GA**, **Kucewicz MT**, **Stein JM**, **Gorniak R**, **Das SR**, **Rizzuto DS**, **Kahana MJ**. Closed-loop stimulation of temporal cortex rescues functional networks and improves memory. *Nat Commun* 9: 365, 2018.

Golabchi A, **Wu B**, **Li X**, **Carlisle DL**, **Kozai TDY**, **Friedlander RM**, **Cui XT**. Melatonin improves quality and longevity of chronic neural recording. *Biomaterials* 180: 225–239, 2018.

Greenberg PE, **Kessler RC**, **Birnbaum HG**, **Leong SA**, **Lowe SW**, **Berglund PAA**, **Corey-Lisle PK**. The Economic Burden of Depression in the United States: How Did It Change Between 1990 and 2000? *J Clin Psychiatry* 64: 1465–1475, 2003.

Guo Z, **Zhang L**, **Wu Z**, **Chen Y**, **Wang F**, **Chen G**. In Vivo Direct Reprogramming of Reactive Glial Cells into Functional Neurons after Brain Injury and in an Alzheimer's Disease Model. *Cell Stem Cell* 14: 188–202, 2014.

Halpern CH, **Samadani U**, **Litt B**, **Jaggi JL**, **Baltuch GH**. Deep Brain Stimulation for Epilepsy. In: *Neuromodulation*. Elsevier, p. 639–649.

Hascup KN, **Hascup ER**, **Stephens ML**, **Glaser PEA**, **Yoshitake T**, **Mathé AA**, **Gerhardt GA**, **Kehr J**. Resting glutamate levels and rapid glutamate transients in the prefrontal cortex of the Flinders Sensitive Line rat: a genetic rodent model of depression. *Neuropsychopharmacology* 36: 1769–77, 2011.

He W, **Bellamkonda R V.** A Molecular Perspective on Understanding and Modulating the Performance of Chronic Central Nervous System (CNS) Recording Electrodes [Online]. CRC Press/Taylor & Francis. http://www.ncbi.nlm.nih.gov/pubmed/21204400 [31 Oct. 2018].

Heinrich C, **Blum R**, **Gascón S**, **Masserdotti G**, **Tripathi P**, **Sánchez R**, **Tiedt S**, **Schroeder T**, **Götz M**, **Berninger B**. Directing Astroglia from the Cerebral Cortex into Subtype Specific Functional Neurons. *PLoS Biol* 8: e1000373, 2010.

Igarashi H, **Koizumi K**, **Kaneko R**, **Ikeda K**, **Egawa R**, **Yanagawa Y**, **Muramatsu S**, **Onimaru H**, **Ishizuka T**, **Yawo H**. A Novel Reporter Rat Strain That Conditionally Expresses the Bright Red Fluorescent Protein tdTomato. *PLoS One* 11: e0155687, 2016.

Jennings JH, **Stuber GD**. Tools for Resolving Functional Activity and Connectivity within Intact Neural Circuits. *Curr Biol* 24: R41–R50, 2014.

Jeong J-W, **McCall JG**, **Shin G**, **Zhang Y**, **Al-Hasani R**, **Kim M**, **Li S**, **Sim JY**, **Jang K-I**, **Shi Y**, **Hong DY**, **Liu Y**, **Schmitz GP**, **Xia L**, **He Z**, **Gamble P**, **Ray WZ**, **Huang Y**, **Bruchas MR**, **Rogers JA**. Wireless Optofluidic Systems for Programmable In Vivo Pharmacology and Optogenetics. *Cell* 162: 662–674, 2015.

Jorfi M, **Skousen JL**, **Weder C**, **Capadona JR**. Progress towards biocompatible intracortical microelectrodes for neural interfacing applications. *J Neural Eng* 12: 011001, 2015.

Karumbaiah L, **Saxena T**, **Carlson D**, **Patil K**, **Patkar R**, **Gaupp EA**, **Betancur M**, **Stanley GB**, **Carin L**, **Bellamkonda R V.** Relationship between intracortical electrode design and chronic recording function. *Biomaterials* 34: 8061–8074, 2013.

Khan W, **Li W**. Wafer level fabrication method of hemispherical reflector coupled micro-led array stimulator for optogenetics. In: *2017 19th International Conference on Solid-State Sensors, Actuators and Microsystems (TRANSDUCERS)*. IEEE, p. 2231–2234.

Konermann S, **Brigham MD**, **Trevino A**, **Hsu PD**, **Heidenreich M**, **Cong L**, **Platt RJ**, **Scott DA**, **Church GM**, **Zhang F**. Optical control of mammalian endogenous transcription and epigenetic states. *Nature* 500: 472–476, 2013.

Kowal SL, **Dall TM**, **Chakrabarti R**, **Storm M V.**, **Jain A**. The current and projected economic burden of Parkinson's disease in the United States. *Mov Disord* 28: 311–318, 2013.

Kozai TDY, **Catt K**, **Li X**, **Gugel Z V.**, **Olafsson VT**, **Vazquez AL**, **Cui XT**. Mechanical failure modes of chronically implanted planar silicon-based neural probes for laminar recording. *Biomaterials* 37: 25–39, 2015a.

Kozai TDY, **Gugel Z**, **Li X**, **Gilgunn PJ**, **Khilwani R**, **Ozdoganlar OB**, **Fedder GK**, **Weber DJ**,

Cui XT. Chronic tissue response to carboxymethyl cellulose based dissolvable insertion needle for ultra-small neural probes. *Biomaterials* 35: 9255–9268, 2014.

Kozai TDY, **Jaquins-Gerstl AS**, **Vazquez AL**, **Michael AC**, **Cui XT**. Brain tissue responses to neural implants impact signal sensitivity and intervention strategies. *ACS Chem Neurosci* 6: 48–67, 2015b.

Kozai TDY, **Jaquins-Gerstl AS**, **Vazquez AL**, **Michael AC**, **Cui XT**. Dexamethasone retrodialysis attenuates microglial response to implanted probes in vivo. *Biomaterials* 87: 157–169, 2016.

Kozai TDY, **Langhals NB**, **Patel PR**, **Deng X**, **Zhang H**, **Smith KL**, **Lahann J**, **Kotov NA**, **Kipke DR**. Ultrasmall implantable composite microelectrodes with bioactive surfaces for chronic neural interfaces. *Nat Mater* 11: 1065–1073, 2012.

Lebedev MA, **Nicolelis MAL**. Brain–machine interfaces: past, present and future. *Trends Neurosci* 29: 536–546, 2006.

Lee M, **Schwab C**, **Mcgeer PL**. Astrocytes are GABAergic cells that modulate microglial activity. *Glia* 59: 152–165, 2011.

Liddelow SA, **Guttenplan KA**, **Clarke LE**, **Bennett FC**, **Bohlen CJ**, **Schirmer L**, **Bennett ML**, **Münch AE**, **Chung W-S**, **Peterson TC**, **Wilton DK**, **Frouin A**, **Napier BA**, **Panicker N**, **Kumar M**, **Buckwalter MS**, **Rowitch DH**, **Dawson VL**, **Dawson TM**, **Stevens B**, **Barres BA**. Neurotoxic reactive astrocytes are induced by activated microglia. *Nature* 541: 481–487, 2017.

Ludwig K a, **Uram JD**, **Yang J**, **Martin DC**, **Kipke DR**. Chronic neural recordings using silicon microelectrode arrays electrochemically deposited with a poly(3,4-ethylenedioxythiophene) (PEDOT) film. *J Neural Eng* 3: 59–70, 2006.

Ludwig KA, **Miriani RM**, **Langhals NB**, **Joseph MD**, **Anderson DJ**, **Kipke DR**. Using a Common Average Reference to Improve Cortical Neuron Recordings From Microelectrode Arrays. *J Neurophysiol* 101: 1679–1689, 2009.

Malaga KA, **Schroeder KE**, **Patel PR**, **Irwin ZT**, **Thompson DE**, **Bentley JN**, **Lempka SF**, **Chestek CA**, **Patil PG**. Data-driven model comparing the effects of glial scarring and interface interactions on chronic neural recordings in non-human primates. *J Neural Eng J Neural Eng* 13: 16010–16024, 2016.

Malone DA, **Dougherty DD**, **Rezai AR**, **Carpenter LL**, **Friehs GM**, **Eskandar EN**, **Rauch SL**, **Rasmussen SA**, **Machado AG**, **Kubu CS**, **Tyrka AR**, **Price LH**, **Stypulkowski PH**, **Giftakis JE**, **Rise MT**, **Malloy PF**, **Salloway SP**, **Greenberg BD**. Deep Brain Stimulation of the Ventral Capsule/Ventral Striatum for Treatment-Resistant Depression. *Biol Psychiatry* 65: 267–275, 2009.

Mayberg HS, **Lozano AM**, **Voon V**, **McNeely HE**, **Seminowicz D**, **Hamani C**, **Schwalb JM**, **Kennedy SH**. Deep Brain Stimulation for Treatment-Resistant Depression. *Neuron* 45: 651–660, 2005.

McCreery D, **Cogan S**, **Kane S**, **Pikov V**. Correlations between histology and neuronal activity recorded by microelectrodes implanted chronically in the cerebral cortex. *J Neural Eng* 13:

036012, 2016.

Michelson NJ, **Vazquez AL**, **Eles JR**, **Salatino JW**, **Purcell EK**, **Williams JJ**, **Cui XT**, **Kozai TDY**. Multi-scale, multi-modal analysis uncovers complex relationship at the brain tissue-implant neural interface: new emphasis on the biological interface. *J Neural Eng* 15: 033001, 2018.

Motta-Mena LB, **Reade A**, **Mallory MJ**, **Glantz S**, **Weiner OD**, **Lynch KW**, **Gardner KH**. An optogenetic gene expression system with rapid activation and deactivation kinetics. *Nat Chem Biol* 10: 196–202, 2014.

Nagy A. Cre recombinase: The universal reagent for genome tailoring. *genesis* 26: 99–109, 2000.

Nolta NF, **Christensen MB**, **Crane PD**, **Skousen JL**, **Tresco PA**. BBB leakage, astrogliosis, and tissue loss correlate with silicon microelectrode array recording performance. *Biomaterials* 53: 753–762, 2015.

O'Doherty JE, **Lebedev MA**, **Ifft PJ**, **Zhuang KZ**, **Shokur S**, **Bleuler H**, **Nicolelis MAL**. Active tactile exploration using a brain-machine-brain interface. *Nature* 479: 228–31, 2011.

Oakes RS, **Polei MD**, **Skousen JL**, **Tresco PA**. An astrocyte derived extracellular matrix coating reduces astrogliosis surrounding chronically implanted microelectrode arrays in rat cortex. *Biomaterials* 154: 1–11, 2018.

Perry VH, **Teeling J**. Microglia and macrophages of the central nervous system: the contribution of microglia priming and systemic inflammation to chronic neurodegeneration. *Semin Immunopathol* 35: 601–12, 2013.

Polikov VS, **Tresco PA**, **Reichert WM**. Response of brain tissue to chronically implanted neural electrodes. *J Neurosci Methods* 148: 1–18, 2005.

Potter KA, **Buck AC**, **Self WK**, **Callanan ME**, **Sunil S**, **Capadona JR**. The effect of resveratrol on neurodegeneration and blood brain barrier stability surrounding intracortical microelectrodes. *Biomaterials* 34: 7001–7015, 2013.

Purcell EK, **Thompson DE**, **Ludwig KA**, **Kipke DR**. Flavopiridol reduces the impedance of neural prostheses in vivo without affecting recording quality. *J Neurosci Methods* 183: 149–157, 2009.

Purcell EK, **Yang A**, **Liu L**, **Velkey JM**, **Morales MM**, **Duncan RK**. BDNF profoundly and specifically increases KCNQ4 expression in neurons derived from embryonic stem cells. *Stem Cell Res* 10: 29–35, 2013.

Ralay Ranaivo H, **Wainwright MS**. Albumin activates astrocytes and microglia through mitogen-activated protein kinase pathways. *Brain Res* 1313: 222–31, 2010.

Rennaker RL, **Miller J**, **Tang H**, **Wilson DA**. Minocycline increases quality and longevity of chronic neural recordings. *J Neural Eng* 4: L1-5, 2007.

Rosin B, **Slovik M**, **Mitelman R**, **Rivlin-Etzion M**, **Haber SN**, **Israel Z**, **Vaadia E**, **Bergman H**. Closed-Loop Deep Brain Stimulation Is Superior in Ameliorating Parkinsonism. *Neuron* 72: 370–

384, 2011.

Rossi JL, **Ralay Ranaivo H**, **Patel F**, **Chrzaszcz M**, **Venkatesan C**, **Wainwright MS**. Albumin causes increased myosin light chain kinase expression in astrocytes via p38 mitogen-activated protein kinase. *J Neurosci Res* 89: 852–61, 2011.

Salatino JW, **Ludwig KA**, **Kozai TDY**, **Purcell EK**. Glial responses to implanted electrodes in the brain. *Nat Biomed Eng* 1: 862–877, 2017a.

Salatino JW, **Winter BM**, **Drazin MH**, **Purcell EK**. Functional remodeling of subtype-specific markers surrounding implanted neuroprostheses. *J Neurophysiol* 118: 194–202, 2017b.

Seidl K, **Spieth S**, **Herwik S**, **Steigert J**, **Zengerle R**, **Paul O**, **Ruther P**. In-plane silicon probes for simultaneous neural recording and drug delivery. *J Micromechanics Microengineering* 20: 105006, 2010.

Seymour JP, **Kipke DR**. Neural probe design for reduced tissue encapsulation in CNS. *Biomaterials* 28: 3594–3607, 2007.

Shen Q, **Rigor RR**, **Pivetti CD**, **Wu MH**, **Yuan SY**. Myosin light chain kinase in microvascular endothelial barrier function. *Cardiovasc Res* 87: 272–80, 2010.

Shen W, **Karumbaiah L**, **Liu X**, **Saxena T**, **Chen S**, **Patkar R**, **Bellamkonda R V.**, **Allen MG**. Extracellular matrix-based intracortical microelectrodes: Toward a microfabricated neural interface based on natural materials. *Microsystems Nanoeng* 1: 15010, 2015.

Sofroniew M V. Molecular dissection of reactive astrogliosis and glial scar formation. *Trends Neurosci* 32: 638–47, 2009.

Sofroniew M V. Astrogliosis. *Cold Spring Harb Perspect Biol* 7: a020420, 2014.

Sofroniew M V, **Vinters H V**. Astrocytes: biology and pathology. *Acta Neuropathol* 119: 7–35, 2010.

Sommakia S, **Lee HC**, **Gaire J**, **Otto KJ**. Materials approaches for modulating neural tissue responses to implanted microelectrodes through mechanical and biochemical means. *Curr Opin Solid State Mater Sci* 18: 319–328, 2014.

Suo Z, **Wu M**, **Citron BA**, **Gao C**, **Festoff BW**. Persistent protease-activated receptor 4 signaling mediates thrombin-induced microglial activation. *J Biol Chem* 278: 31177–83, 2003.

Tong M, **Hernandez JL**, **Purcell EK**, **Altschuler RA**, **Duncan RK**. The intrinsic electrophysiological properties of neurons derived from mouse embryonic stem cells overexpressing neurogenin-1. *Am J Physiol Physiol* 299: C1335–C1344, 2010.

Vierbuchen T, **Ostermeier A**, **Pang ZP**, **Kokubu Y**, **Südhof TC**, **Wernig M**. Direct conversion of fibroblasts to functional neurons by defined factors. *Nature* 463: 1035–1041, 2010.

Volterra A, **Meldolesi J**. Astrocytes, from brain glue to communication elements: the revolution continues. *Nat Rev Neurosci* 6: 626–640, 2005.

Weaver FM, **Follett K**, **Stern M**, **Hur K**, **Harris C**, **Marks WJ**, **Rothlind J**, **Sagher O**, **Reda D**, **Moy CS**, **Pahwa R**, **Burchiel K**, **Hogarth P**, **Lai EC**, **Duda JE**, **Holloway K**, **Samii A**, **Horn S**, **Bronstein J**, **Stoner G**, **Heemskerk J**, **Huang GD**, **Group for the C 468 S**, **KA F**, **S M**, **J C**, **RL R**, **F W**, **AE L**, **Y T**, **P K**, **G D**, **MM H**, **JW L**, **MF F**, **S F**, **RS S**, **V P**, **RA H**, **CG G**, **R P**, **A S**, **K S-T**, **H J**, **P L**, **K W**, **M A**, **BS A**, **Y T**, **KJ B**, **MI H**. Bilateral Deep Brain Stimulation vs Best Medical Therapy for Patients With Advanced Parkinson Disease<subtitle>A Randomized Controlled Trial</subtitle> *JAMA* 301: 63, 2009.

Weinstein JR, **Gold SJ**, **Cunningham DD**, **Gall CM**, **Sastre A**, **Lyuboslavsky P**, **Hepler JR**, **McKeon RJ**, **Traynelis SF**. Cellular localization of thrombin receptor mRNA in rat brain: expression by mesencephalic dopaminergic neurons and codistribution with prothrombin mRNA. *J Neurosci* 15: 2906–19, 1995.

Wellman SM, **Eles JR**, **Ludwig KA**, **Seymour JP**, **Michelson NJ**, **McFadden WE**, **Vazquez AL**, **Kozai TDY**. A Materials Roadmap to Functional Neural Interface Design. *Adv Funct Mater* 28: 1701269, 2018.

Wimo A, **Jönsson L**, **Bond J**, **Prince M**, **Winblad B**, **Alzheimer Disease International**. The worldwide economic impact of dementia 2010. *Alzheimers Dement* 9: 1–11.e3, 2013.

Winter B, **Daniels S**, **Salatino J**, **Purcell E**. Genetic Modulation at the Neural Microelectrode Interface: Methods and Applications. *Micromachines 2018, Vol 9, Page 476* 9: 476, 2018.

Winter BM, **Setien MB**, **Salatino JW**, **Blanke N**, **Thompson CH**, **Smith KR**, **Khan WA**, **Li W**, **Suhr ST**, **Purcell EK**. Control of cell fate and excitability at the neural electrode interface: Genetic reprogramming and optical induction. In: *2017 IEEE Life Sciences Conference (LSC)*. IEEE, p. 157–161.

Zamanian JL, **Xu L**, **Foo LC**, **Nouri N**, **Zhou L**, **Giffard RG**, **Barres BA**. Genomic analysis of reactive astrogliosis. *J Neurosci* 32: 6391–410, 2012.